LBL-10916 c.2
Preprint

Lawrence Berkeley Laboratory
UNIVERSITY OF CALIFORNIA

Accelerator & Fusion
Research Division

Submitted to the Journal of Applied Physics

HIGH CURRENT D^- PRODUCTION BY CHARGE EXCHANGE IN SODIUM

E.B. Hooper, Jr., P. Poulsen, and P.A. Pincosy

February 1981

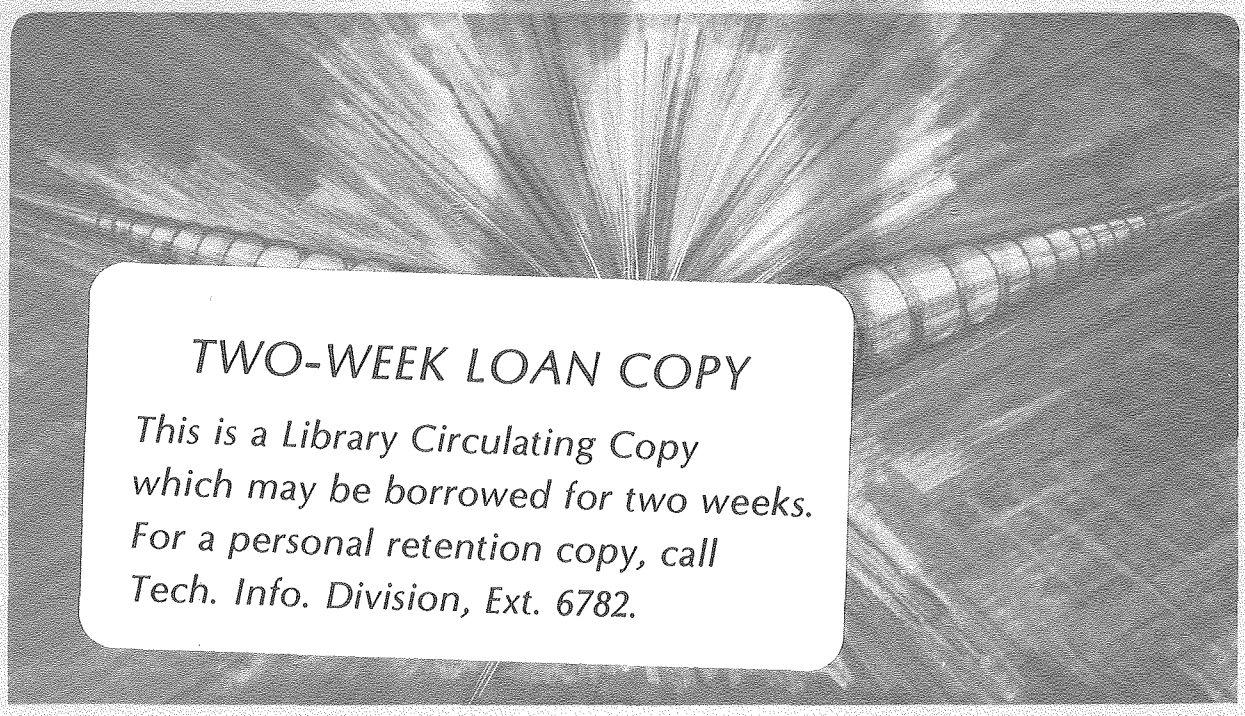

Prepared for the U.S. Department of Energy under Contract W-7405-ENG-48

DISCLAIMER

LBL-10916

High Current D^- Production by Charge Exchange in Sodium*

E. B. Hooper, Jr.**
P. Poulsen**
P. A. Pincosy**

Lawrence Berkeley Laboratory
University of California
Berkeley, California 94720

February 26, 1981

* This work was supported by the Director, Office of Energy Research, Office of Fusion Energy, Development and Technology Division, of the U. S. Department of Energy under Contract No. W-7405-ENG-48.

** Permanent Address: Lawrence Livermore National Laboratory, Livermore, CA. 94550.

ABSTRACT

A beam of D^- ions has been produced at 7-13 keV, with currents up to 2.2 A, using charge exchange in sodium vapor. The beam profile is a bi-Gaussian with angular divergence 0.8° x 2.7° and peak current density 15 mA/cm^2. The characteristics of the beam are in excellent agreement with predictions based on atomic cross sections. The sodium vapor target is formed by a jet directed across the beam. The sodium density drops rapidly in the beam-line downstream from the charge exchange region; decreasing three orders of magnitude in 15 cm. Measurement and analysis of the plasma accompanying the beam demonstrate that plasma densities nearly equal to the beam density are obtained one meter from the charge exchange medium. The plasma produced in the sodium is thus well confined to the charge exchange region and does not propagate along the beam.

INTRODUCTION

The generation of efficient, very high energy, neutral beams of the isotopes of hydrogen is generally believed to require the use of negative ions.[1,2] Positive ions are difficult to neutralize: For deuterions at 200 keV for example, the efficiency of neutralization by charge exchange in deuterium is 20 percent, and it decreases rapidly at higher energies.[2] However, the stripping of an electron from the negative deuterium ion is about 60 percent efficient at 200 keV and even greater stripping efficiencies can be obtained in plasmas[3] or in intense light beams.[4] Given this information, it is straightforward to show that neutral beams based upon negative ions are potentially a highly efficient means of obtaining plasma heating in thermonuclear experiments and reactors.[1,5,6]

A general beam line based on negative ions consists of a source of negative ions, an accelerator, a stripper to convert the negatives to neutral atoms, and a means for handling the residual beam ions either by dumping them on cooled surfaces or (preferably) by recovering their energy. The status of this work is reviewed in Ref. 7; see also Ref. 8.

Essential to any system, of course, is the source of negative ions. Many different sources have been proposed and studied.[9] The approaches tested include charge-exchange in alkali metals,[10-16] production on surfaces,[17-19] production in the volume of a plasma,[20,21] and others.

This report describes the production of a D^- beam by charge exchange in sodium. Up to 2.2 A have been produced in a well directed beam, with a bi-Gaussian angular distribution, typically 0.7° x 2.8° and with energy 7-13 keV. The data is in excellent agreement with calculations using measured cross sections, thus demonstrating that no significant "anomalous" processes are important in the production and transport of the D^- beam.

I. BACKGROUND FOR THE EXPERIMENT

The exchange of electrons between ionic and/or neutral particles is an important process on the atomic scale. In the formation of beams, for example, it is used to change a high energy proton or deuteron beam into a neutral (atomic and molecular) beam.[2] The evolution of species in a beam versus the density of the charge exchanging gas vapor through which the beam propagates was analyzed by Allison.[22] Tarawa and Russek[23] summarized data for hydrogen beams, and a complete summary of data may be found in the ORNL compilation.[24] Hooper and Willmann[25] have analyzed the angular scattering of a beam during the charge exchange process.

The cross sections for electron capture by hydrogen or deuterium atoms in alkali metal vapors are large at energies in the keV range.[22-24] At these energies, the equilibrium fraction of negative ions in a beam can be as large as 35 percent; Schlachter et al have summarized the measurements.[26-28]

The first experiment which used charge exchange to produce negative ion currents high enough to be of interest for neutral beam production was that of Osher et al.[10] They passed a 1 keV, deuteron beam through cesium and produced 50 mA of D^-. This was extended to 300 mA by Hooper, et al.[11,12] They accelerated 100 mA of this current to 60 keV, demonstrating good beam optics and control of electrons. In cesium, however, it is difficult to obtain good beam optics at the 1 keV energy and below required for efficient conversion. Experimental and theoretical analysis of this problem was done by Orzechowski,[29] who obtained a 10 A, deuteron beam with divergence 2.0° x 7.5°. Further work using cesium is also planned by Geller and coworkers,[30,31] and by the group at Karlsruhe.[32,33]

Charge exchange of large beams in sodium has been studied by Semashko and co-workers[13,14] and by the present authors.[15,16] The maximum conversion efficiency[26-28] in sodium (11 percent at 3 keV for D^0) is less than in

cesium (35 percent at 0.5 keV for D^0), but the sodium efficiency remains high to relatively high energies. This permits operation at energies at which beam optics is good. At these higher energies the angular scattering of the charge-exchanging beam is also weaker. Thus, a higher quality beam is obtained although at the cost of a lower total current.

II. Apparatus

The experiment was performed on the LBL Test Stand I, shown in Fig. 1. A positive ion beam produced at one end of the system propagated through the charge exchange jet, a diagnostic chamber, and onto a beam dump.

The positive ion source was a 7 cm x 35 cm pulsed source of the type known as "LBL-50 Amp",[34] and is discussed in the next section. The source was followed by a neutralizer which largely converted the positive ions to neutrals and dissociated many of the molecular ions. Pulse lengths of 10 ms were used to keep gas pulses in the beam line low.

On the time scale of the beam pulse the vacuum pressures were determined by the tank volumes and conductances. The gas input into the source tank, typically 19 Tl/s, was thus well isolated from the rest of the system by apertures and by the gas impedence of the sodium jet. Similarly, gas evolution from the beam dump/calorimeter was isolated from the diagnostic tank by apertures in order to prevent stripping of the negative ions. Estimates using the volumes and conductances, and measurements using fast ion gages, both yielded a pressure of 2×10^{-5} Torr in the diagnostic region at the end of a beam pulse. Further discussion can be found in Appendix A.

Charge exchange targets for use in large aperture beamlines are usually formed by a jet of metal vapor directed across the particle beam. The non-isotropic velocity distribution of a jet reduces the flow along the beamline and directs the flow across the beamline to a pump. Our pump consists of

condensation surfaces. If the vapor is not localized, it may adversely affect the performance of the beam accelerators and the target plasma for which the beam is generated.

The charge exchange cell used in this experiment is shown schematically in Fig. 2. A jet of sodium atoms was formed by an external expansion nozzle (illustrated in Fig. 3.) which effectively directed the metal vapor. The density profile of sodium through the vapor target was measured by a hot wire probe. Results for the design condition (line density = nL = 2×10^{15} cm^{-2}) are shown in Fig. 4. It is seen that the sodium is well localized, with the density decreasing three orders of magnitude in 15 cm. The sodium collected on surfaces downstream was measured by neutron activation, yielding fluxes at 80 cm from beam center of 4×10^{-4} that at the center. This nozzle configuration thus succeeds in preventing a large flux of charge exchange vapor along the beamline.

Inside the charge exchange vacuum tank there is a secondary enclosure for the sodium or other alkali metal, termed the "warm-box". The warm box houses the nozzle and a funnel shaped collector. During operation sodium evaporates from the boiler and passes through the superheater to a valve attached to the nozzle. The valve is actuated pneumatically from outside the enclosure, typically for 0.5 second or less. The sodium escaping from the nozzle freezes out on the collector; when required the collector is heated above the melting point of the metal which then flows back into the boiler for reuse. The warm box has two roles: to contain any sodium which misses the collector and to act as a secondary container when the sodium is recycled. During the latter operation the doors to the warm box are closed so that vapor cannot escape. The liquid from the collector (or elsewhere in the charge exchange cell) drains into the warm box, e.g. through a hole in the bottom of the collector. A valved tube leads from the bottom of the warm box to the boiler. Further

details of the jet design and charge exchange operation are found elsewhere.[16,36]

Diagnostics used in this experiment are indicated by number in Fig. 1. They included: (1) ion gauges which could be operated using fast electronics (1 ms response time); (2) a calorimeter to determine the total beam power and beam profile; (3) a bending magnet which could eliminate the charged particle part of the beam before the beam reaches the calorimeter; (4) a scanning Faraday cup to measure the (net) current density in the beam, (5) a scanning magnetic analyzer to measure the D^- current density; (6) Langmuir probes to measure plasma density and temperature; and (7) a scanning hot wire probe to measure the sodium flux. Signals from Langmuir probes in the positive ion sources were telemetered from the high voltage cage.

III. POSITIVE ION BEAM

The positive ion source and accelerator producing the beam for this experiment has been used extensively.[34] The accelerator consists of 105 slots, each 2 mm x 7 cm. The grids wires are bowed along their length to provide a focus at 3.0 m from the source. Focusing in the direction across the grids is provided by offsetting the grid at the plasma surface from those downstream; the focus is also at 3.0 m in this direction. Typical operation was at 10.5 kV and required 25 A of accelerator power supply drain.

From calorimeter measurements of the total beam and from Faraday cup measurements of the ion part of the beam, we found that the beam angular divergence parallel to the slots was $0.75^\circ \pm .05^\circ$ at 10 keV. As the transverse energy in the plasma source depends only weakly on source operation, the angular divergence will scale as $E_b^{-\frac{1}{2}}$, where E_b is the beam energy.

Across the slots the angular divergence is sensitive to the match between space charge and the electric field. As a result, the minimum angular divergence occurs for a fixed perveance; the optimum was found to be at an accel current of $I = 0.74\ V^{3/2}$ A, with the voltage in kV. At 10.5 keV, the beam angular divergence in the direction across the slots was 2.75° ± 0.05°; this also scales as $E_b^{-\frac{1}{2}}$.

The beam composition has been measured by Stearns,[2] and data from various source operations compiled by Cooper.[37] Their results are close to those obtained at the Kurchatov Institute in a similar source.[38] We conclude that our initial beam has the following fractional composition:

$$f(D^+) = 0.60 \pm 0.05;\ f(D_2^+) = 0.30 \pm 0.05;\ f(D_3^+) = 0.10 \pm 0.02. \qquad (1)$$

There is also a low level of impurity (< 3 percent of oxygen); this will be discussed in a later section.

The source was operated with a standard "neutralizer" following the accelerator. The gas impedence of this duct, 8 cm x 37 cm x 41 cm (long) is sufficient to provide a D_2 line density of approximately 5×10^{15} cm^{-2} along the beam. The beam composition is consequently changed, both in charge state and molecular composition, in passing through the neutralizer. The final composition was calculated using known cross sections.[2] Results are given in Table 1 for 10 keV.

IV. NEGATIVE DEUTERIUM PRODUCTION

The production of D^- was studied as a function of sodium density and as a function of beam energy. To describe the process we proceed by first considering the negative ion beam at a fixed energy, 10.5 keV. This analysis

demonstrates that the production can be explained by known atomic cross-sections and that the spreading of the beam by collisions is small, and provides a detailed description of the process. On considering the production as a function of beam energy and taking into account the variation of the positive ion beam, we show that the negative ion beam scales as predicted.

As a guide to understanding the data, we note that the breakup of molecular deuterium ions in sodium requires a line density comparable to or greater than 10^{16} cm^{-2}.[39] Thus, at our sodium densities (10^{15} cm^{-2}) it is a good approximation when predicting the negative ion production to neglect the molecular components of the beam which reach the sodium cell. This differs from the results of Semashko et al.[13,14]; they typically operate at $> 5 \times 10^{15} cm^{-2}$ and thus dissociate much of the molecular component of the beam.

A. Fixed Beam Energy

Measurements at 10.5 keV, Fig. 5, show the current densities at the beam center. The magnetic analyzer measures the D^- current density, and the Faraday cup measures the net current density: $D^+ - D^-$ + impurity ions. The beam pulse length was 10 ms; the time dependences at sodium line densities $nL = 0$ and $nL = 1 \times 10^{13}$ cm^{-2} are shown in Fig. 6. Spatial beam profiles are shown in Fig. 7 (along the direction of the source slots) and Fig. 8 (across the slots). The profile of D^- is only slightly broader than that of positive ions, indicating that angular scattering is weak; see Appendix B for details.

The difference between the net current and the D^- current is primarily due to the positive deuterium ions. It is plotted in Fig. 9. Except for very low line densities it can be fit quite well by an exponential with decay corresponding to a cross section $\sigma = 7.5 \times 10^{-15}$ cm^2. Measurements by Anderson et al.[46] yield $\sigma_{+0} = (6.1 \pm 1.5) \times 10^{-15}$ cm^2 at 10 keV

(D^+), with only weak dependence on energy, thus confirming that the dominant process is $D^+ + Na \longrightarrow D + Na^+$.

Fig. 9 also shows the total positive current density predicted from that at the neutralizer exit of the source. The molecular ions are about 20 percent of this value.

The lack of drop-off at low values of $n\ell$, observed in the figure, will also be seen in the D^- signal. It arises from an error in the conversion from sodium density measurements to the line density due to changes in the axial profile at low sodium density.

In calculating the negative ions we neglect the contribution from molecular ions entering the charge-exchange cell as their dissociation is small at the sodium line densities used in this experiment. We predict the current density of D^- to be:

$$j_- = j_T \sum_{a=1}^{3} f_a \left\{ F_-^\infty - (F_-^\infty - F_-^0) \exp\left[- \sigma_{0-} + \sigma_{-0}) nL \right] \right\}_a \qquad (2)$$

with j_T the total current density of single nucleus deuterium and f_a the fractional composition of the a-th energy component. The values of the cross sections σ_{-0} have been measured by Howald et al.[41]; F_-^∞ has been measured by Schlachter[26-28] and by Anderson et al.[40]; their results are in excellent agreement in the energy range of interest. The formation cross sections are found from $\sigma_{0-} = \sigma_{-0} F_-^\infty / (1-F_-^\infty)$.

The total current density is found from the acceleration power supply drain (25 A for these data), the angle of the well directed part of the beam, 0.85% $\pm$ 0.6%, and the bi-Gaussian widths (0.75 °× 2.77°). We obtain $j_T = 0.17 \pm .01$ A/cm^2 at the detector location in the diagnostic tank. The resulting negative ion current densities are plotted in Fig. 10. An uncertainty of 7 percent has been attributed to the prediction, corresponding to the uncertainty

in the well directed part of the positive ion current. The error bars do not include errors in cross sections (uncertain) and in F_-^∞ ($\pm$ 5 percent).[26-28]

The data is also plotted on Fig. 10. A typical error bar of $\pm$ 10 percent is shown, arising from two uncertainties: (a) The area of the entrance aperture and orientation of the analyzer ($\pm$ 6 percent), and the uncertainty in the suppression of secondary electrons and background plasma in the magnetic analyzer ($\pm$ 4 percent).

The agreement is quite good, thus indicating that the model of production and propagation of the D^- beam is accurate. The data, however, show a fall-off with line density. Although the fall-off is within the accuracy of the measurement, it is systematic thus suggesting that it is real. The reason for the fall-off is not understood; we will show in later sections that angular scattering and plasma effects are not large enough to explain it.

B. Production as a Function of Energy

The production at various energies was measured and compared with the predictions. The results are shown in Fig. 11. Note that the efficiency is expressed in terms of the total acceleration current; in terms of the well directed current, the efficiencies would be $(0.85)^{-1} = 1.18$ times higher. The total current produced is plotted in Fig. 12. Although the efficiency of production decreases with increasing energy, the total available current increases as the 1.5 power of the beam voltage; this dominates the drop off in efficiency and increases the total D^- current. Also, the source can be operated at currents somewhat above the optimum perveance, at the cost of an increase in beam divergence. Using this technique, 2.2 A of D^- were obtained in a 0.75° x 3.0° bi-Gaussian at an acceleration voltage of 12 kV.

C. Beam Impurity Content

The current density of negative impurities in the beam is of concern both because they represent a drain on any power supply required for post acceleration and because a large fraction of the impurities could be injected into the reactor plasma.

The magnetic (momentum) analyzer had a Faraday cup to collect heavy negative ions. However, the field was not strong enough to separate them significantly from the neutral component of the beam, and secondary effects from these particles (surface electrons, gas ionization, etc.) masked the signal of interest and prevented reliable measurements. From the increase in signals on this cup when the sodium jet is operated, we estimate about 10 percent negative impurity content, albeit with a low confidence level in the accuracy.

Another estimate of the impurity level can be made. The primary impurity is expected to be oxygen, accelerated as OD^+ and originating at walls in the source. Spectroscopic measurements[42] indicate approximately 2 percent impurity. Measurements of radiation from the 2XIIB mirror machine extrapolate to a 1-3 percent oxygen impurity in the beams.[43] This was the primary high energy, impurity radiation observed, and therefore undoubtedly the primary impurity found in the beams. Finally, after the D^- experiments our source was run with helium[44]; the acceleration power supply current was about 7 percent higher than that predicted from operation with deuterium. The space charge effects scale as the square root of the species mass, so this is consistent with a 3 percent oxygen impurity in the deuterium beam which is absent in the helium beam. It is thus plausible to assume an upper limit of oxygen of 3 percent in the primary beam.

The conversion of O^+ to O^- in sodium has been measured by Heinemeier and Hvelplund[45] and by Nagata[46]. From these measurements we estimate that the

maximum conversion efficiency is less than 0.4, and occurs at an energy between 10 and 15 keV.

The conversion efficiency is less than this at a sodium line density of 10^{15} cm^{-2}. Nagata's results indicate that at 5 keV and below, a line density of more than 10^{16} cm^{-2} is required to reach a full equilibrium value of O^-. From Ref. 45 we estimate that a thickness of 8×10^{15} cm^{-2} is required to reach equilibrium at higher energies. If we take this to be three e-folds, at $nL = 10^{15}$ cm^{-2} (as required to fully convert the deuterium) the conversion of oxygen to O^- is roughly 10 percent. As the conversion efficiency of deuterium is 8.5 percent, we estimate the ratio of O^- to D^- to be about $0.03 \times 0.10/0.085 = .035$. Thus, the impurity level in the D^- beam is predicted to be approximately the same as in the initial D^+ beam.

V. PLASMA EFFECTS

A. Introductory Comments

The charged and neutral beams produce a plasma by direct collisions by the beam particles (and secondary plasma particles) with background gas and the vapor in the charge-exchange cell. This plasma, in turn, has a number of effects which can have major effects on propagation and the utility of the negative ions:

(1) The plasma provides space-charge neutralization of the beam; without this the beam would blow up in a very short distance.

(2) The negative ions may be destroyed by charge exchanging collisions with plasma (positive) ions.

(3) A beam plasma instability may generate a strong enough radio-frequency electric field to disrupt beam propagation.

(4) Ionization of the sodium (or other charge exchange vapor) coupled with plasma transport may enhance vapor losses from the cell.

(5) Electrons from the plasma may enter a post-accelerator, causing an appreciable power drain and problems associated with high energy electrons.

In this section we describe the results of measurements of the secondary plasma temperature and density, compare these with our calculations, and discuss the implications of these results.

B. Experimental Results

Measurements were made using a Langmuir probe in the diagnostic tank and another probe on the downstream edge of the charge exchange jet. Both probes were shielded from direct bombardment by the beam particles and the jet probe had a guard ring to protect against sodium deposits. Typical results are shown in Table 2. The densities were estimated from the ion current using simple Langmuir probe theory[47] and then corrected using the theory of Hall and Freis,[48] which is based on orbit calculations of the ion motion.

Several features are noteworthy:

(1) The plasma density in the diagnostic tank increased only slightly as a result of the sodium jet operation. As discussed later, the ion loss rate is predicted to be proportional to $T_e^{\frac{1}{2}}$, and the measurements very nearly have constant $i_+ T_e^{-\frac{1}{2}}$ providing evidence that the ion species is the same whether the sodium jet is on or off.

(2) Measured plasma densities in the diagnostic tank are larger by a factor of about 3 than the density of the charged ions in the beam.

(3) The presence of sodium reduces the measured value of T_e from 5 to 10 eV to between 1.0 and 1.5 eV near the cell.

(4) There is an electron temperature gradient between the cell and the diagnostic tank when the sodium jet is operating.

The plasma density in the diagnostic tank was measured across the narrow dimension with the results shown in Fig. 13. A final set of measurements are

presented in Fig. 14 in which the plasma density in the charge-exchange cell is plotted versus the sodium density.

B. Plasma Model and Comparison with Results

Calculations of beam density profiles in ion beams have been done for both one and two dimensional geometry using a fluid equation model.[49,50] As a first approximation we note that our beams are much narrower in one traverse direction (~5 cm) than in the other (~14 cm) so that the beam can be approximated as a slab. The one-dimensional continuity equation can be solved simultaneously with the ion momentum equation.[50] For the case in which the beam space charge is small, the density is

$$n/n_w = \left\{1 + \left[1 - F(x)/n_w\right]^2\right\}^{\frac{1}{2}} \tag{3}$$

with n_w, the density outside the beam, equal to $F(\infty)$; in the slab approximation this remains constant to the wall. Also,

$$F(x) = \frac{1}{c_s} \int_0^x S_i(x)\, dx \tag{4}$$

with S_i the source of ions and c_s is the speed of sound for the plasma ions, $\sqrt{kT_e/M_i}$.

For a Gaussian beam with half width R_b to the 1/e point, F(x) is an error function with an upper limit at high ionization rates

$$n_w = \frac{\sqrt{\pi}\, n_0}{2\, c_s}\, S_{i0} \tag{5}$$

with S_{i0} the value of S_i at x = 0. For the case of the negative beam, the ion density will approach the beam density at low ionization rates.

The total cross sections for production of D_2^+ in D_2 have been summarized by Barnett, et al.[23] At 10 keV, we have $\sigma_1 \approx 8.5 \times 10^{-16}$ cm^2 for collisions with charged beam particles and $\sigma_2 \approx 0.4 \times 10^{16}$ cm^2 for those with neutrals. The cross sections for forming D^+ are much smaller. Our beams typically contain 10 percent D^+ or D^-; the effective cross section is $\sigma_1 + \sigma_2 n_b^0/n_b^+ \approx 1.25 \times 10^{-15}$ cm^2. We use this value for both positive and negative beams.

Positive sodium ions can be produced both by charge exchange and by ionization. The cross section for charge exchange has been measured by Howald et al.[41]; for 10 keV deuterium $\sigma_{-0} = 3.25 \times 10^{-15}$ cm^2. They and Schlachter[51] have both measured $F_-^\infty = 0.072$; from $F_-^\infty = \sigma_{0-}/(\sigma_{-0} + \sigma_{-0})$, we find $\sigma_{0-} = 2.5 \times 10^{-16}$ cm^2. A similar value is estimated from the data used in measurements by Schlachter.[51] The cross section also can be estimated from calculations by Janev and Radulovic[52]; extrapolating their results from 5 keV to 10 keV, we find $\sigma_{0-} = 8 \times 10^{-17}$ cm^{-2}. The higher experimental values are used.

The cross sections for ionization of sodium are not known. O'Hare et al.[53] have measured the cross section for $H^+ + Na \rightarrow H^+ + Na^+ + e$ at 20 keV and above. They also summarize calculations by numerous authors to energies as low as 3 keV. From their results we estimate $\sigma \approx 1.3 \times 10^{-15}$ cm^2 for D^+ at 10 keV. We also use this for ionization by D^-. The cross section for ionization by D^0 is presumably smaller.

Because the neutral part of the beam is much greater than the ion part, the dominant process generating Na^+ is charge exchange: $D^0 + Na \rightarrow D^- + Na^+$. In sodium, at equilibrium for 10 keV, the D^0 to D^- density ratio is $n_b^0/n_b^- = 14$, so the charge exchange production of positive ions,

normalized to the negative ion density, is $\sigma_+ = \sigma_{0-}\, n_b^0/n_b^- \approx \sigma_{-0} = 3.25 \times 10^{-15}$ cm^{-2}; including ionization we obtain $\sigma_+ = 4.5 \times 10^{-15}$ cm^2.

The ratio of ionization by electrons to that by the beam is

$$r = \frac{\langle \sigma v \rangle_e \quad n_e}{\sigma_+ \; v_b \; n_b} \tag{6}$$

In deuterium gas, at $T_e = 5$ eV, the ionization rate by electrons is $\langle \sigma v \rangle_e = 10^{-10}$ cm^3/sec; for the beam the ionization rate is $\sigma^0_{+b} = 1.2 \times 10^{-7}$ cm^3/sec. Clearly the beam dominates for the case of $n_b \approx n_e$.

In the sodium jet the plasma density is much greater than the beam density. To estimate the ratio r, we treat it as an expansion, using the result $n = 2n_w$ and Eq. 3 to yield

$$r = \sqrt{\pi}\, \langle \sigma v \rangle_e \, R_b n_0 / c_s \tag{7}$$

The ionization rate in sodium is found in Ref. 54. Measurements (Table 2) range from $T_e = 1$ eV with $\langle \sigma v \rangle_e = 4.8 \times 10^{-10}$ cm^3/sec to 1.5 eV with $\langle \sigma v \rangle_e = 3.4 \times 10^{-10}$cm^3/sec just downstream of the jet. Using our beam parameters, Eq. 7 yields $r = 1.1 \times 10^{-14}\; n_0$ at $T_e = 1$ eV and $r = 7.8 \times 10^{-14}\; n_0$ at $T_e = 1.5$ eV so that the electron ionization will become important at sodium densities, n_0, between 1.3×10^{13} cm^{-3} and 9×10^{13} cm^{-3}. Note, however, that this assumes a fully developed tail on the Maxwellian; depletion of this tail by excitation will raise the density at which ionization by electrons becomes important. Estimates of this effect[16] indicate an increase to roughly 8×10^{14} cm^{-3} for electrons to become an important source of ionization.

Next consider these results in the diagnostic region where ionization rates are low. The density at x = 0 is predicted to be

$$n \lesssim \frac{\sqrt{\pi} n_0}{c_s R_b} \sum_{\substack{\text{beam} \\ \text{species}}} v_+^{(i)} \sigma_b^{(i)} n_b^{(i)} \qquad (8)$$

Assuming that the plasma is predominately D_2^+, created in D_2 by a 10 keV D^+ beam, we find

$$n/n_b \approx 1.5 \times 10^4 \, p/\sqrt{T_e} \qquad (9)$$

with p the pressure in torr. We measure $p = 3 \times 10^{-5} T$ and $T_e = 5$ eV and thus predict $n/n_b \approx 0.2$. The measured density is an order of magnitude higher. The reason for this discrepancy at low ionization rates is not known. A similar effect was seen for a 1 keV beam generated in cesium,[49] although the cross sections are not as well known and the effect therefore not as clear.

The plasma density in the charge exchange cell requires a two dimensional calculation because of the short axial extent of the sodium profile. It was modeled by the Plasflow code,[50] a two dimensional, fluid equation model with the electron density given by a Maxwell-Boltzmann distribution. The sodium density was assumed uniform across the beam and varied along the beam with the measured profile. Downstream the sodium density was given a value scaled from the positive ion production cross sections (above), using the measured gas pressure; the resulting profile is shown in Fig. 14. The axial electron temperature variation was not included; T_e was set to 1 eV everywhere.

The end conditions are important for this calculation. Modeling them is difficult: at a wall the velocity equals or exceed the speed of sound, but there is gas evolution where the beam strikes. Rather than attempt to describe this, the ion velocity was given a "floating" boundary condition at the wall, $\partial v_z/\partial z = 0$.

In these calculations, the beam was assumed rigid and of fixed (negative) charge along the system:

$$n_b = 1.40 \times 10^9 \exp\left[-(x/3.5)^2\right] \text{ cm}^{-3} \tag{10}$$

Results of the calculation are shown in Fig. 15 - 18. Several points are noteworthy:

(a) As seen in Fig. 15 the plasma has not reached its asymptomatic value at 200 cm although in the experiment the downstream density is 3.3×10^9 cm^{-3} at z = 80 cm. On these long scale lengths the beam is not well represented by the infinitely wide model of the calculation; the flow to the walls will be enhanced by the expansion arising from transverse flow.

(b) At z = 24 cm and x = 4.5 cm, the code predicts $n = 8.0 \times 10^{10}$ cm^{-3}; this is good agreement with the measured value of 1.1×10^{11} cm^{-3} at 25 cm.

(c) In Fig. 16 we note that T_z shows two regions in which it increases. In the region from 10 to 20 cm the increase is due to ionization and is shown in Ref. (50) to have only a small effect. Downstream where compressional heating occurs, T_z becomes large and affects the flow significantly. Because the axial sound velocity is $\left[(T_e + T_z)/M_i\right]^{1/2}$, the rapid increase in T_z causes the flow to become sonic rapidly (after supersonic flow) and thus strongly effects the dynamics.

(d) We note in Fig. 17 that the transverse density profile is quite flat even though the beam space charge is small. This is because the plasma generated upstream has a large component of transverse flow and contributes significantly to the off-axis density.

C. Consequences of the Plasma

As discussed at the beginning of this section, the plasma generated in the charge exchange cell has several consequences:

(1) Space charge neutralization. As the plasma density is (typically) 500-1000 times the beam density, space charge neutralization in the charge-exchange cell is complete. The transverse potential drop approximately equals the electron temperature, 1 eV, and thus causes a negligible beam perturbation.

(2) Charge exchange destruction of D^-. The cross section for this process, has been calculated by Janev and Radulovic[52] to be $\sigma_{cx} = 4.0 \times 10^{-15}$ cm^{-2}. A simple calculation shows that the negative equilibration fraction is $F_-^\infty = \sigma_{0-} \left[\sigma_{0-} + \sigma_{-0} + \sigma_{cx}\, n_+/n_0\right]^{-1}$. Using $\sigma_{0-} = 2.5 \times 10^{-16}$ cm^2, $\sigma_{-0} = 3.25 \times 10^{-15}$ cm^2, and $n_+/n_0 = 10^{-2}$, we find $\left[\sigma_{cx}\, n^+/n_0\right] / \left[\sigma_{0-} + \sigma_{-0}\right] = 1.1 \times 10^{-2}$. Thus, even if considerable error exists in the cross sections and the plasma density calculations and measurements, charge exchange losses of D^- on Na^+ are negligible.

(3) Beam plasma instability. Measurements yielded no evidence of instability. The detector (probe) technique was sensitive to 10 MHz.

(4) Transport of sodium by plasma effects. No careful measurements were made. However, the two dimensional calculations (above) indicate that most of the sodium ions flow to the walls in a distance of order of the beam thickness.

(5) Downstream plasma effects. The downstream ratio of random electron current to (deuterium) beam current is $1.7\ (n/n_0)\ \sqrt{T_e/E_b}$. At the measured density ratio of about 2, the current ratio is 0.75, too large to be acceptable in a negative ion accelerator. It appears, therefore, that although the plasma density has been greatly reduced by plasma flow an auxiliary means of suppressing electrons may be required if the beam is to be accelerated.

VI. CONCLUSIONS

A well directed beam of 2.2A of D^- has been produced by charge exchange in sodium. Predictions using known properties of sources together with atomic cross sections yield good agreement between predictions and the measurements.

Gas flow and production throughout the beamline was predictable and controllable, as discussed in Appendix A.

Sodium loss from the charge exchange cell is small due to the nozzle and cell geometry used in the experiment. Plasma produced in the sodium cell is shown not to extend far downstream, in agreement with calculations.

Because of these results, scaling of the beam to sizes of interest for the production of high energy neutral beams can be undertaken with confidence. Such an analysis will be undertaken elsewhere.

ACKNOWLEDGEMENTS

We would like to thank R. V. Pyle and the rest of the LBL-MFE neutral beam group for their hospitality during the course of this work.

This work was supported by the Director, Office of Energy Research, Office of Fusion Energy, Development and Technology Division, of the U. S. Department of Energy under Contract No. W-7405-ENG-48.

Appendix A: GAS EFFECTS IN BEAMLINE

It is essential to keep the pressure of gas low in the propagation region for negative ions because of their large stripping cross section,[24] $1.2 \times 10^{-15} cm^2$ for 10 keV D^- in D_2. Gas is produced by four mechanisms: flow through the source, production when the beam is stopped in the beam dump, evolution from surfaces along the beamline which are stuck by particles in the beam fringes, and evolution from diagnostics placed in the beam.

During the initial operation of the experiment, large amounts of gas were generated from bombardment of warm, stainless steel surfaces near the exit of the charge-exchange cell which were coated with sodium. Because the exit aperture was large (20 cm x 50 cm) the flow into the diagnostic tank was rapid, leading to a linear increase of pressure with time. Measurements by a residual gas analyzer determined that the primary gases involved were H_2 and D_2.

The gas problem was eliminated by two measures:

(a) The aperture between the source tank and the charge-exchange cell was reduced in size from the original 20 cm x 50 cm to 7.5 cm x 36 cm by inserting a copper plate. This reduced the total current by only 2 percent, "trimmed" any highly divergent, non Gaussian wings, and thus reduced bombardment of downstream surfaces. The reduced aperture also reduced gas flow from the source tank into the charge exchange cell.

(b) Stainless steel surfaces which could be struck by fringe beams were protected by copper plates as gas evolution can be substantial from stainless steel.[58] These plates were thermally isolated so that heating due to radiation from the nozzle would minimize the build-up of sodium on their surfaces.

With these measures the gas pressure in the diagnostic tank was below 3×10^{-5} T during the beam pulse, with the primary source of gas in the

diagnostic region that generated in the beam dump tank. Using the known tank volume (600 L) and conductance between the two tanks (10 cm x 40 cm aperture), it was estimated that the gas evolution rate (nuclei per second) during 10 ms beam pulse was at about twice the impact rate for beam particles (nuclei per second).

Anderson[57] and Semashko et al.[14] have pointed out that the sodium jet acts as a barrier for the flow of gas from the source region to the downstream region. For a sodium line density of 2.5×10^{15} cm^2, Semashko, et al. obtained pressure differences across their jet of 15 for H_2 and 60 for D_2. In this experiment the pressure in the diagnostics tank was measured early in a gas pulse (no beam). During this period the pressure in the diagnostic tank was proportional to the conductance through the tank. The increase with the jet was 0.52 of that with the jet off; the conductance (jet off) was measured to be 2.0×10^3 L/sec. Given a jet cross section area of 1400 cm^2, we find $C_{jet} = 1.6$ L/cm^2sec. This was less than estimated from simple considerations. From a simple diffusion model, we find $C = 10^{-3}$ $v/3\sigma nL$ with the deuterium thermal velocity $v = 8 \times 10^4$cm/sec at 300 K, nL the sodium line density, and σ the deuterium-sodium cross section. Scaling from cesium[57] by the relative atomic sizes, we estimate $\sigma = 4 \times 10^{-15}cm^2$, so that $C = 6.7 \times 10^{15}/nL$ L/cm^2-sec. At the temperature of boiler operation (545 C), $nL = 1.35 \times 10^{15}cm^{-2}$, so we estimate C = 5 L/cm^2-sec, about three times the measured value.

The reason for the more favorable measurement is not known. It may arise from the directed motion of the D_2 resulting from the jet character; this gives a downward pumping effect[14] which will reduce the gas flow.

Appendix B. ANGULAR SCATTERING

Angular Scattering during charge-exchange processes has been measured by Cisneros et al.[58] in cesium and by Agafonov et al.[59] in both cesium and sodium. Hooper et al.[60] have described the effect of angular scattering on the F_-^∞ measurements of Schlachter et al. in cesium.[26-28]

These results yield an average scattering angle which can be modeled by

$$\theta_s = K(R^2/R_{Na}^2)(nL)^\alpha/E \qquad (B1)$$

with R the crystal lattice dimension; we have normalized to sodium. Note that R = 4.24 Å for sodium and 6.05 Å for cesium. As is typical for scattering effects, the "reduced scattering angle", $E\theta$, is an approximate reduced variable.[61]

The dependence on line density can be predicted in several limits. Thus, if θ_s is determined by many small, elastic scatterings, the angle increases by diffusion in velocity space and one expects $\alpha = 0.5$. Conversely, if elastic scattering is unimportant at small line densities, θ_s will equal the average scattering angle associated with the neutral to negative charge-exchange process.[25] At moderate line densities it will increase linearly and finally at large line densities multiple collisions will lead to $\alpha = 0.5$.

The measurements of Agafonov et al.[61] yield $\alpha = 0.70 \pm .07$ for the cases of D^+ + Cs (0.5 kV); H^+ + Cs (6 kV); and H^+ + Na (4 kV). These results also yield an approximate inverse energy dependence, although the data for D^+ + Cs at 1 keV and below indicates a weaker dependence ($E^{-0.32}$). In this range, Cisneros et al.[58] show a dependence of $E^{-0.7}$ for multiple scatterings.

Values of K are listed in Table 3. In the cases of Agafonov et al.[54] the angle θ_s is defined in terms of the broadening of the half-height of the current distribution. That of Cisneros et al. is defined as the cone angle within which 50 percent of the D^- is formed.

The measurements of Schlachter were not performed with the purpose of obtaining angular scattering data, so only a rough estimate of the scattering angle is possible.[60] By assuming that the scattering decreases the current density illuminating the exit aperture we estimate the value given in the table.

Semashko et al.[14] quote an increase angular divergence of 0.15° for 5 keV H^- ions as nL increased by 1 x 10^{15} cm^{-2}. This corresponds to the K = 0.75 in the table.

Because the angular scattering was small in our experiment, no attempt was made to study it systematically. The one pertinent observation was that at E = 10.5 keV and nL = 1.35 x 10^{15} cm^{-2}, the half-width at 1/e of the negative ion current distribution (along the slots) was W_1 = 0.28 cm wider than the D^+ profile (W_0 = 2.76 cm). Defining the scattering angle as $\theta_s = (W_1^2 - W_0^2)^{\frac{1}{2}}/L_1$, with L_1 = 80 cm the distance from the center of the charge-exchange jet, we find θ_s = 0.91 and K = 7.8. This result is so much larger than any of the other results that it seems likely that it has arisen from some mechanism other than angular scattering. It might, for example, reflect the difference in species origin (D^+, D_2^+, or D_3^+) of the residual D^+ and the D^-.

The beam current density will not be significantly reduced by scattering of the magnitude measured by Agafonov, et al.[59] and by Cisneros et al.[58] We conclude that angular scattering is not significant in our experiment.

References

1. A. C. Riviere, Neutral Injection Heating of Toroidal Reactors, Culham Report CLM-R112 (1971), Appendix 3.
2. K. H. Berkner, R. V. Pyle, and J. W. Stearns, Nucl Fusion 15, 249 (1975).
3. G. I. Dimov and G. V. Rosylakov, Nucl. Fusion 15, 551 (1975).
4. J. H. Fink and A. M. Frank, LLL Report UCID-16844 (1975).
5. E. B. Hooper, Jr.,Proc. 3rd Symp. Plasma Heating in Toroidal Devices, E. Sindoni, ed. (Editorial, Bologna, 1976), p. 278.
6. J. F. Fink,Proc. Symp. and Neut. of Negative Hydrogen Ions and Beams, K. Prelec, Ed. (Brookhaven, 1977), p. 290.
7. E. B. Hooper, Jr., IEEE Trans. Nucl. Sci. NS-26, 1287 (1979).
8. See Proc. Symp. Prod. and Neut. Negative Hydrogen Ions and Beams, K. Prelec, ed. (Brookhaven, 1977).
9. E. B. Hooper, Jr., LLL Report UCID-18067 (1979).
10. J. E. Osher, F. J. Gordon, and G. W. Hamilton, Proc. 2nd Intl. Ion Source Conf., Vienna, 1972.
11. P. Poulsen, O. A. Anderson, E. B. Hooper, Jr., T. J. Orzechowski, and R. J. Turnbull, Proc. 7th Symp. Eng. Prob. Fusion Research, 1408 (1977).
12. E. B. Hooper, Jr., O. A. Anderson, T. J. Orzechowski, and P. Poulsen, Ref. 8, p. 163.
13. N. N. Semashko, V. V. Kusnetsov, and A. I. Krylov, Ref. 8, p 170.
14. N. N. Semashko, V. V. Kuznetsov, and A. I Krylov, Proc. 8th Symp. Eng. Prob. Fusion Research, (1979).
15. P. Poulsen and E. B. Hooper, Jr., Proc. 8th Symp. Eng. Prob. Fusion Research, (1979).
16. E. B. Hooper, Jr., P. Poulsen, P. A. Pincosy, O. A. Anderson, and T. J. Duffy, Lawrence Berkeley Laboratory Report LBL-10454 (1980).
17. Yu. I. Bel'chenko, G. I. Dimov, and V. G. Dudnikov, Ref. 8, p 129.

18. K. Prelec, Ref. 8, p 111.

19. K. W. Ehlers and K.-N. Leung, to be published.

20. M. Bacal, E. Nicolopoulou and H. J. Doucet, Ref. 8, p. 26.

21. M. Bacal and G. W. Hamilton, Phys. Rev. Letters 42, 1538 (1977).

22. S. K. Allison, Rev. Mod. Phys. 30, 1137 (1958).

23. H. Tarawa and A. Russek, Rev. Mod. Phys. 45, 178 (1973).

24. C. F. Barnett, J. A. Ray, E. Ricci, and M. I. Wilker, "Atomic Data for Controlled Fusion Research," ORNL-5206 (1977).

25. E. B. Hooper, Jr. and P. A. Willmann, J. Applied Phys. 48, 1041 (1977).

26. A. S. Schlachter, K. R. Stalder, and J. W. Stearns, Proc. 10th Intl. Conf. Phys. Elec. and Atomic Coll., Paris, 1977, p. 870.

27. A. S. Schlachter in Ref. 8, p 11.

28. A. S. Schlachter, K. R. Stalder, and J. W. Stearns, submitted to Phys. Rev. A.

29. T. J. Orzechowski, unpublished.

30. R. Geller, C. Jacquot, and P. Sernet, Ref. 8, p 173.

31. R. Geller, B. Jacquot, C. Jacquot, P. Sernet, and J. Tsheros, to be published.

32. W. B. Becker, H. D. Falter, O. F. Hagnea, W. Henkes, R. Klingelhofer, H. Moser, W. Obert, and J. Roth, Ref. 8 p 322.

33. E. B. Becker, H. D. Falter, O. F. Hagena, W. Henkes, R. Klingelhofer, H. Moser, W. Obert, and I. Poth, Nucl. Fusion 17, 617 (1799).

34. W. R. Baker, K. H. Berkner, W. S. Cooper, K. W. Ehlers, W. B. Kunkel, R. V. Pyle, and J. W. Stearns, Plasma Physics and Controlled Fusion Research, 1979, (IAEA, Vienna, 1975), Vol I, 329.

35. P. Poulsen, G. H. Ratekin, T. J. Duffy, Bull Am. Phys. Soc. (1978).

36. P. Poulsen, to be published.

37. W. S. Cooper, III, unpublished.

38. N. N. Semashko, private communication.

39. A. S. Schlachter, unpublished.

40. C. J. Anderson, A. M. Howald, and L. W. Anderson, Nucl. Instr. Meth. 165, 583 (1979).

41. A. M. Howald, L. W. Anderson, and C. C. Liu, Bull. Am. Phys. Soc. 24, 1186 (1979).

42. C. F. Burrell, unpublished

43. P. Drake and H. W. Moos, Nucl. Fusion, 19, 407 (1979).

44. E. B. Hooper, Jr., P. A. Pincosy, P. Poulsen, C. F. Burrell, L. Grisham, and D. E. Post, Rev. Sci. Instr.

45. J. Heinemeier and P. Hvelplund, Nucl. Instr. Meth., 148, 425 (1978).

46. T. Nagata, J. Phys. Soc. Japan 46, 919 (1979).

47. F. Chen, R. H. Huddlestone and S. L. Leonard (ed) Plasma Diagnostic Techniques (Academic Press, New York, 1965), Chapter 4.

48. L. S. Hall and R. Freis, Proc. 7th Intl. Conf. Phen. Ionized Gases, Vol. III, 15 (1966).

49. O. A. Anderson and E. B. Hooper, Jr., Proc. Symp. Prod. and Neutr. of Negative Hydrogen Ions and Beams, K. Prelec, Ed., (Brookhaven, 1977), p. 205.

50. E. B. Hooper, Jr., O. A. Anderson, and P. A. Willmann, Phys. Fluids 22, 2334 (1979).

51. A. S. Schlachter, private communication. The experiment was not designed to measure cross-sections, so the estimate of cross sections is accurate to within a factor of two, at best.

52. R. K. Janev and Z. M. Radulovic, Phys. Rev. A, 17, 889 (1978).

53. B. G. O'Hare, R. W. McCullough, and H. B. Gilbody, J. Phys. B., Atom. Phys. 8, 2968 (1975).

54. W. Lotz, Astrophys. J. Suppl. XIV, 107 (1967).

55. S. A. Self, J. Appl. Phys. 36, 456 (1965).

56. H. Haselton, private communication.

57. O. A. Anderson, Lawrence Livermore Laboratory Report UCID-16914 (1975).

58. C. Cisneros, I. Alvarez, C. F. Barnett, and J. A. Ray, Phys. Rev. A14, 76 (1976).

59. Yu. A. Agafonov, B. A. D'yachkov, and M. A. Pavlii, J. Tech. Phys, to be published.

60. E. B. Hooper, P. A. Willmann, and A. S. Schlachter, UCID-17726 (1978).

61. E. Everhart, Phys. Rev. 132, 2083 (1963).

Table I. Beam composition at exit of neutralizer. Initial composition: $D^+ = 0.6$; $D_2^+ = 0.3$; $D_3^+ = 0.1$. Beam energy = 10 keV; initial ion current = 1A; neutralizer (D_2) line density = $5 \times 10^{15} cm^{-2}$.

Species	Energy 10.keV	6.7 keV	5 keV	3.3keV	Sum
D^0	.530	---	.348	.129	1.007
D^+	.062	---	.040	.015	.117
D^-	.008	---	.002	.0005	.0105
D_2	.095	.045	---	---	.140
D_2	.010	.004	---	---	.014
D_e^+	.019	---	---	---	.019

Table II. Typical Probe Measurements

PROBE			PLASMA			ASSUMED
Radius	Length	Location	Ion Density	Electron Temperature	Sodium Jet	ION SPECIES
3.8×10^{-2} cm	0.70 cm	Diagnostic Tank, Beam Center	2.6×10^{9} cm^{-3}	4.5 eV	Off	D^+
3.8×10^{-2} cm	0.7 cm	Diagnostic Tank, Beam Center	3.3×10^{9} cm^{-3}	2.6 eV	On NL = 1.0×10^{15} cm^{-2}	D^+
3.8×10^{-2}	1.0 cm	Charge-Exchange	1.1×10^{11} cm^{-3}	1.5 eV	On NL = 1.5×10^{15} cm^{-2}	Na^+

Table III. Angular scattering coefficient. The units of K are deg - keV $-(10^{15}cm^2)^{-0.7}$.

Ion	Vapor	E	N	K	Reference Comments
D	Na	2-5	2.2×10^{15}	0.16	Agafonov[54]
H	Na	2-4	$0.4 - 5 \times 10^{15}$	0.14	Agafonov[54]
D	Cs	0.5-1	$0.5 - 1.7 \times 10^{15}$	0.13	Agafonov[54]
H,D	Cs	1.2-5	1.1×10^{15}	0.11	Agafonov[54]
D	Cs	0.5-2.5	8×10^{14}	0.15	Cisneros[53]
D	Cs	0.5-3	1×10^{15}	0.18	Hooper[55] - rough estimate
H	Na	5	1×10^{15}	0.75	Semashko[14]
D	Na	10.5	1.35×10^{15}	7.8	This work. Not verified to be due to scattering.

Figure Captions

1. Test Stand 1. The positive ion source was followed by a neutralizer tube, resulting in a D_2 line density $5 \times 10^{15} cm^{-2}$ along the beam.
2. Charge exchange cell.
3. External flow nozzle used to form the sodium jet.
4. Sodium profile for $nL = 2 \times 10^{15}$ cm^{-2}.
5. Net current and D^- current as a function of sodium line density, nL. Beam acceleration voltage 10.5 kV.
6. Oscilloscope traces of the beam. (a) Positive ions (nL=0) and (b) negative ions ($nL = 1 \times 10^{15}$ cm^{-2}).
7. Negative beam profile parallel to the beam slots.
8. Positive, neutral, and negative beam profiles across the beam slots.
9. Dependence of positive current on sodium line density, nL.
10. Predicted and measured current density of D^-.
11. Conversion efficiency of positive to negative ions (D^-) as a function of beam acceleration voltage.
12. Total negative ion (D^-) current as a function of beam acceleration voltage. Operation at differing source perveances (and angular divergences) is shown.
13. Plasma ion density profile across the beam: measured in the diagnostic tank with the jet off.
14. Plasma ion density in the charge-exchange cell as a function of sodium density.
15. Assumed sodium density and predicted plasma density profiles along the beam axis.
16. Ion axial velocity, v_z, and stress, T_z, along the beam axis.
17. Transverse beam ion density and plasma densities at z = 0, 24, and 100 cm.
18. Transverse beam ion velocities at z = 0, 24, 100 cm.

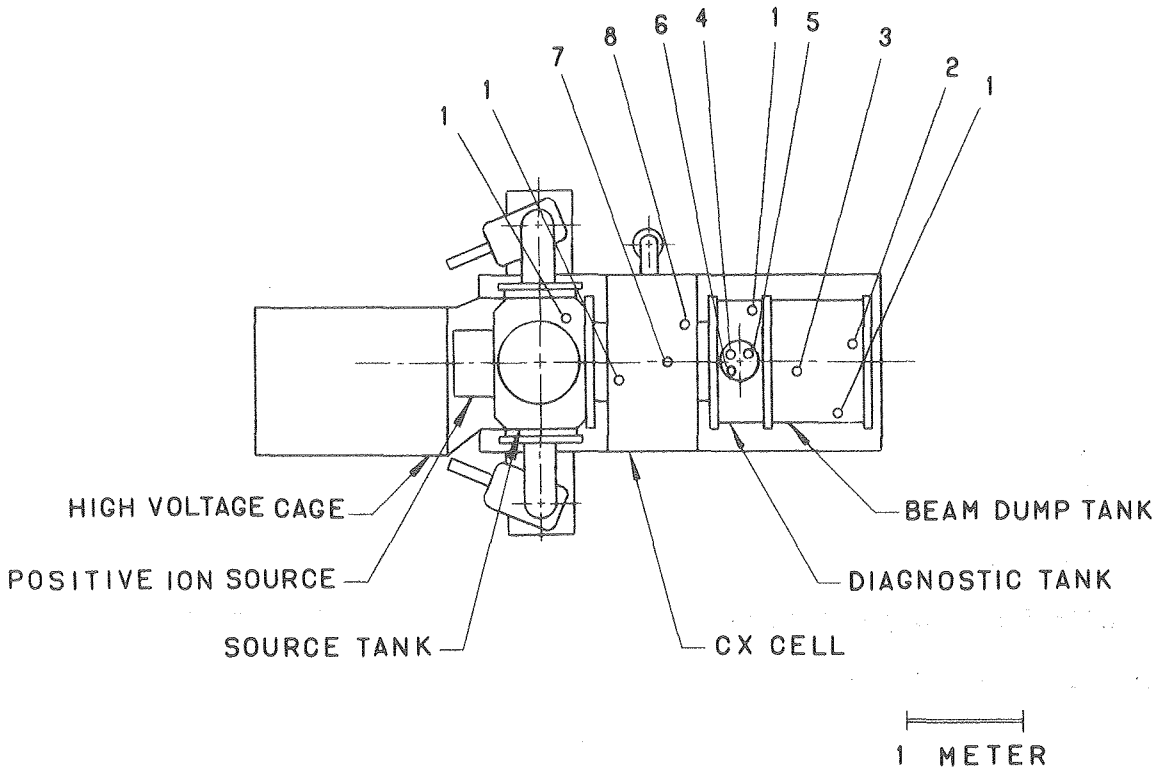

XBL 803-8831

Fig. 1

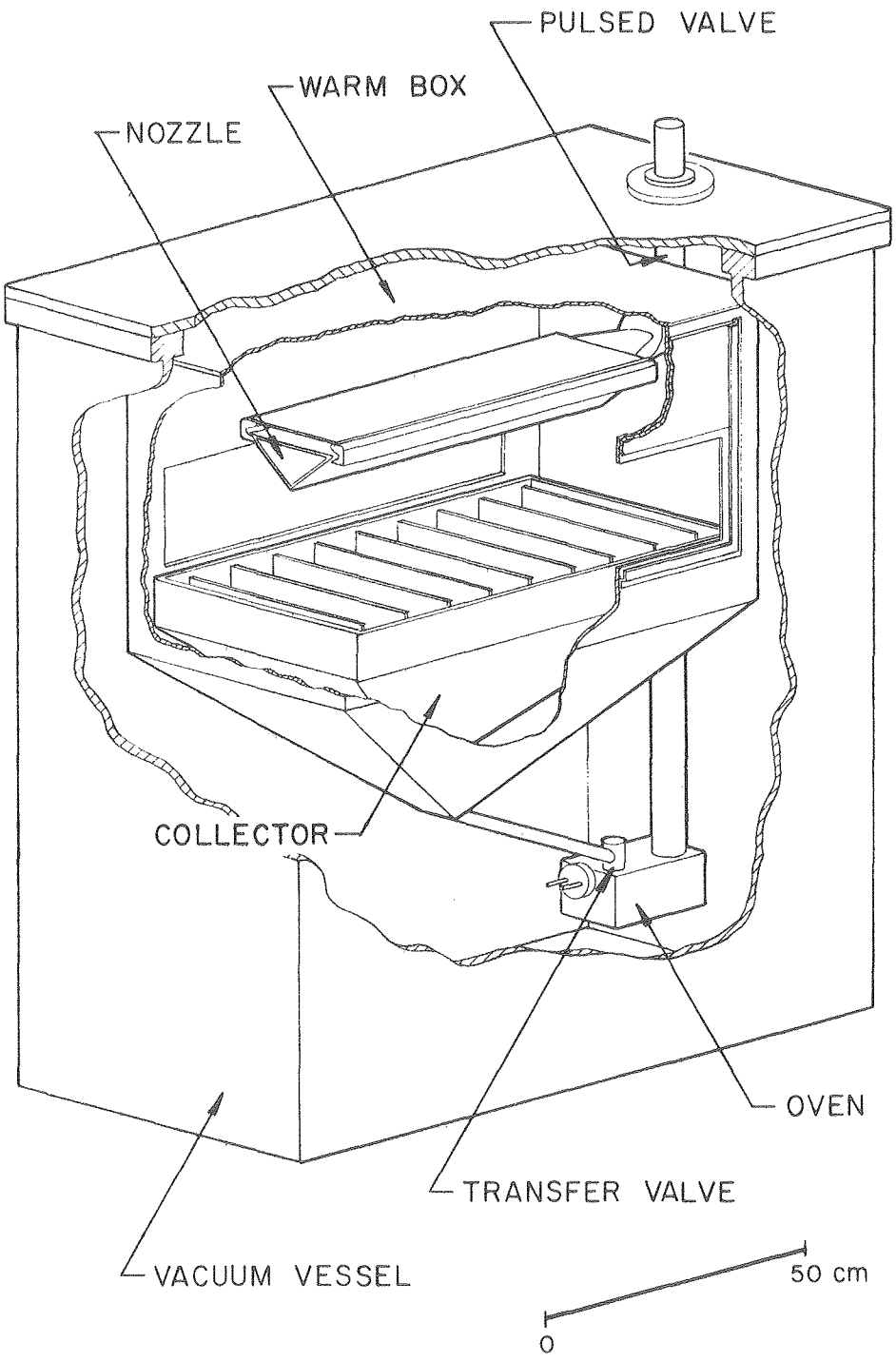

XBL 809-11826

Fig. 2

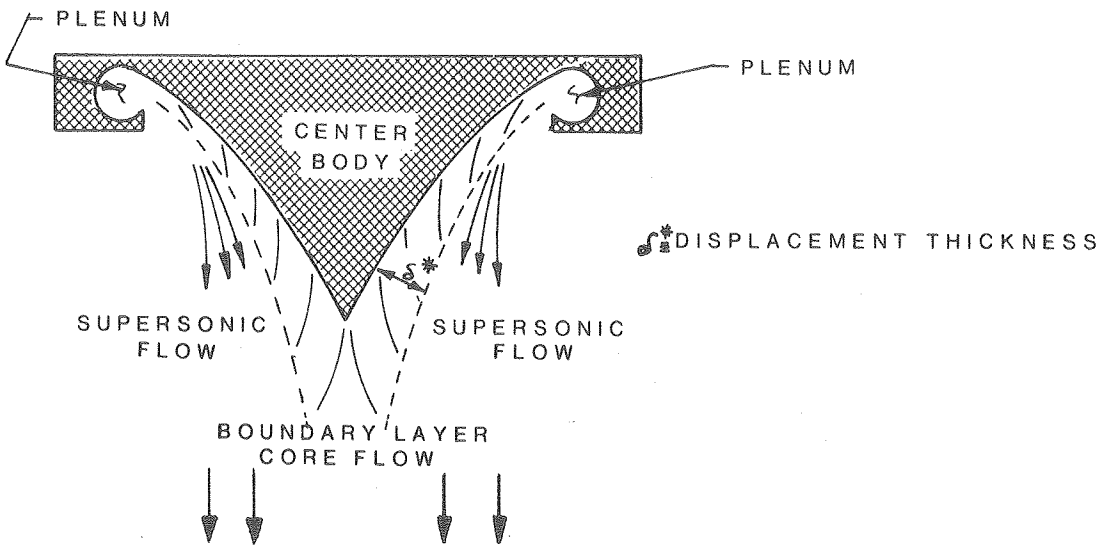

XBL 812-8085

Fig. 3

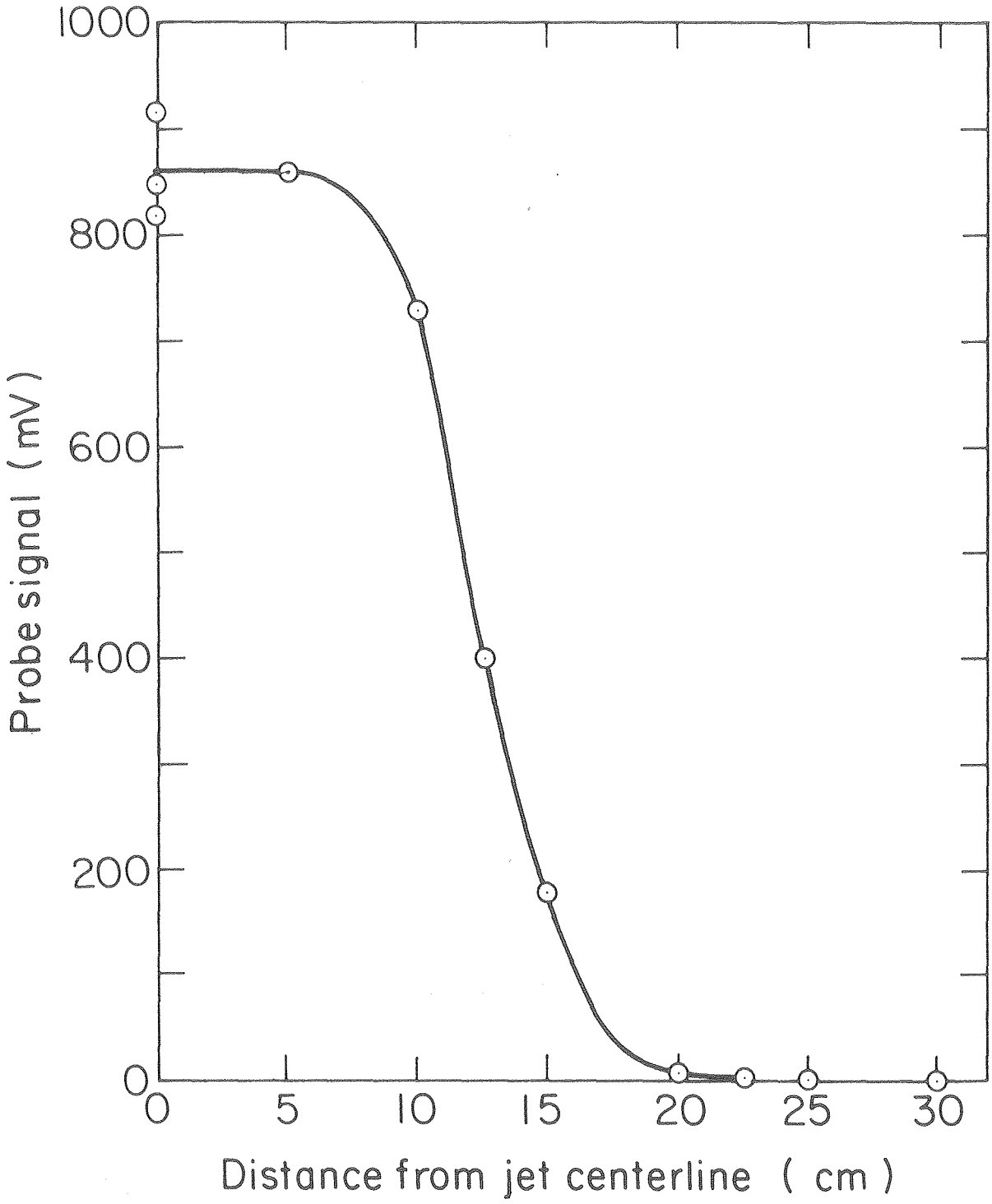

Fig. 4

XBL 805-1001

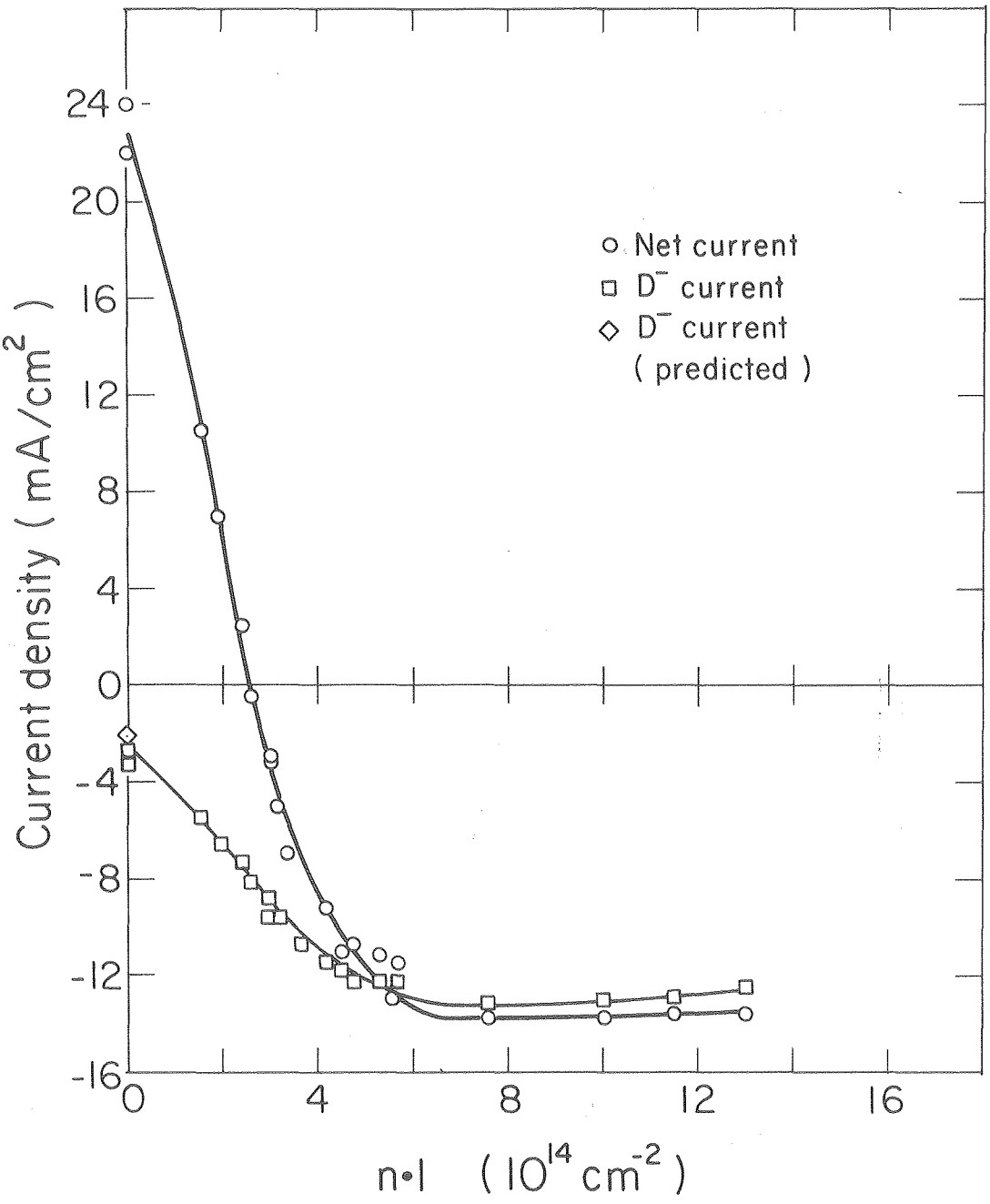

Fig. 5

XBL806-1025

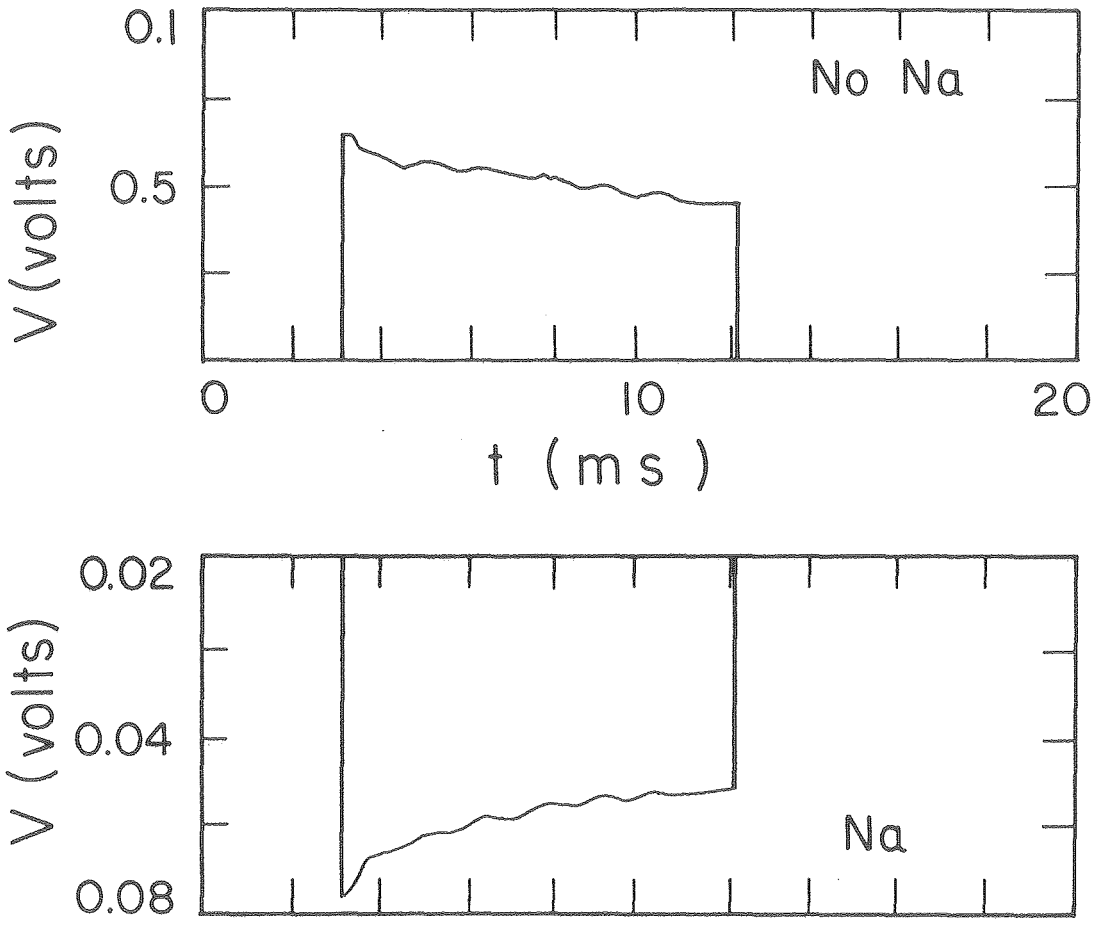

Fig. 6

XBL809-1922

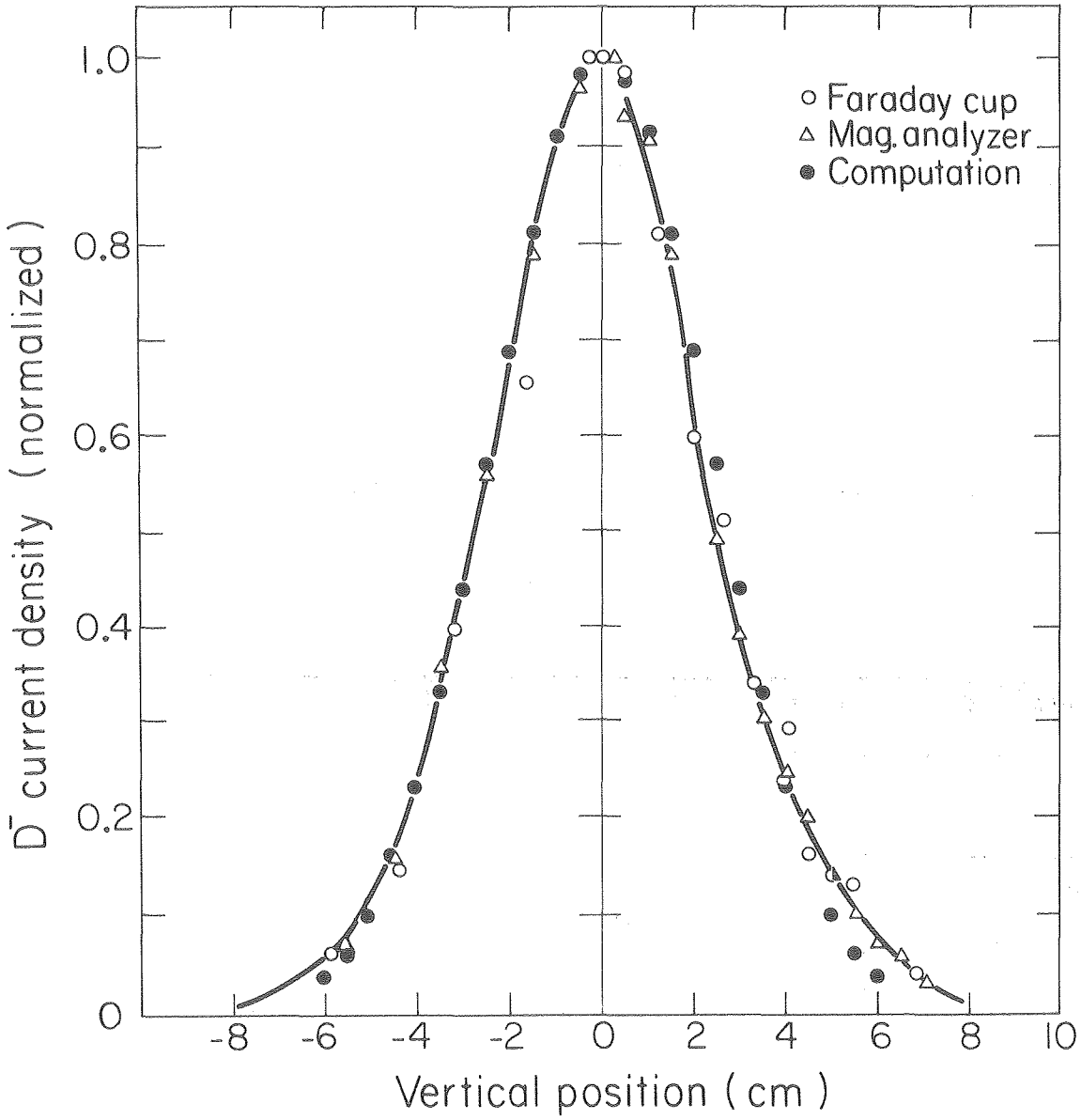

Fig. 7

XBL 806-1019

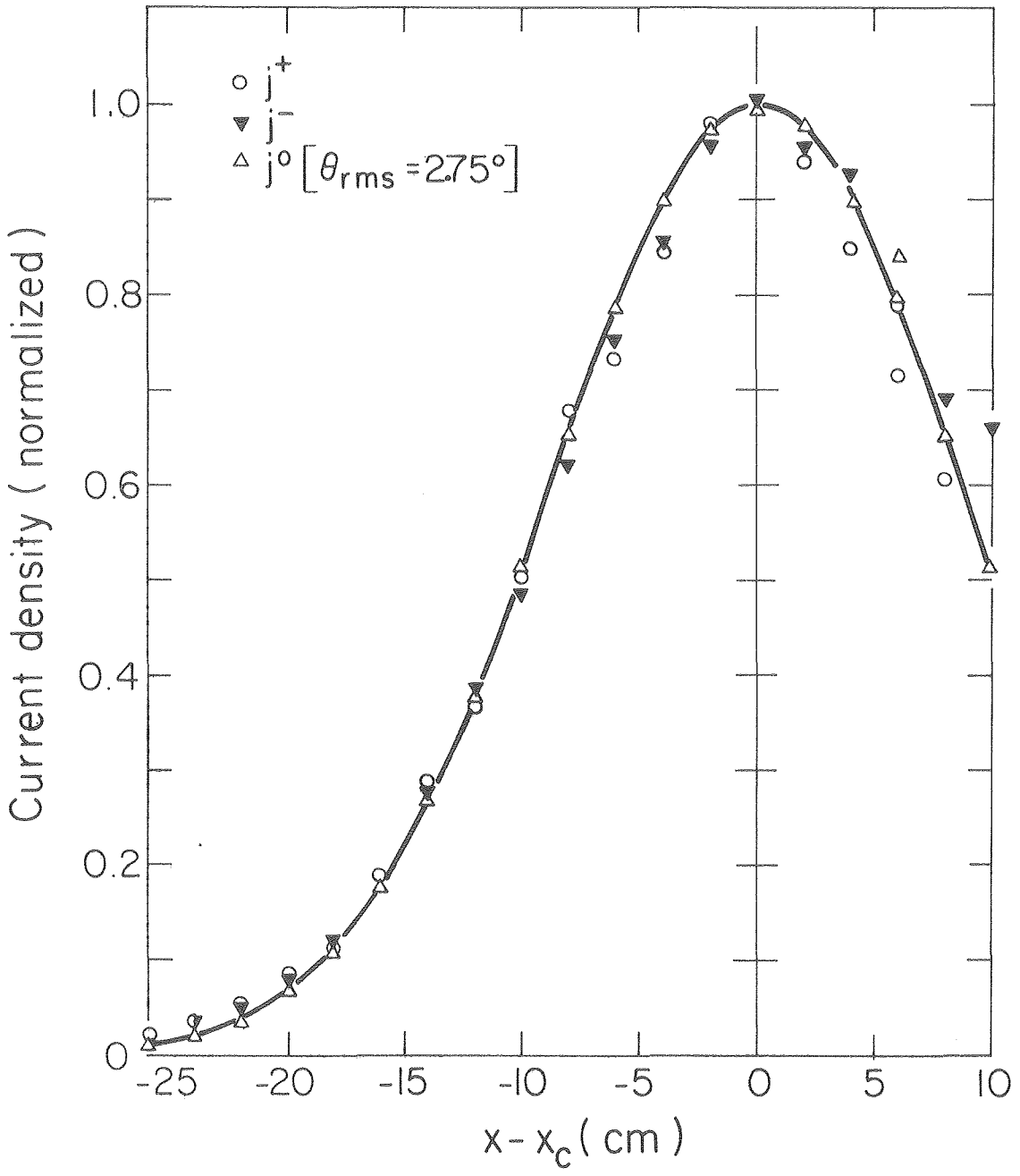

XBL806-1018

Fig. 8

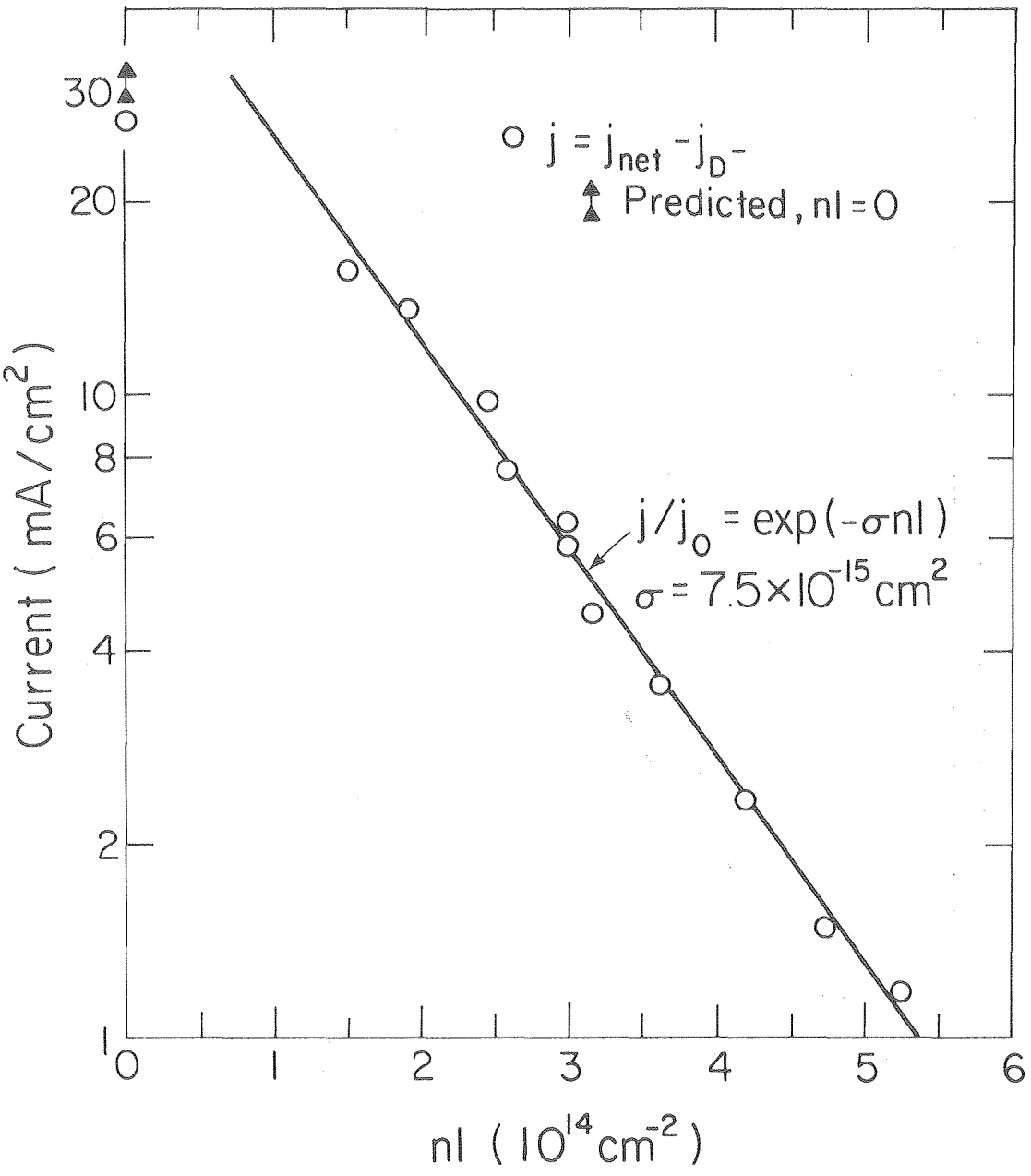

XBL 806-1024

Fig. 9

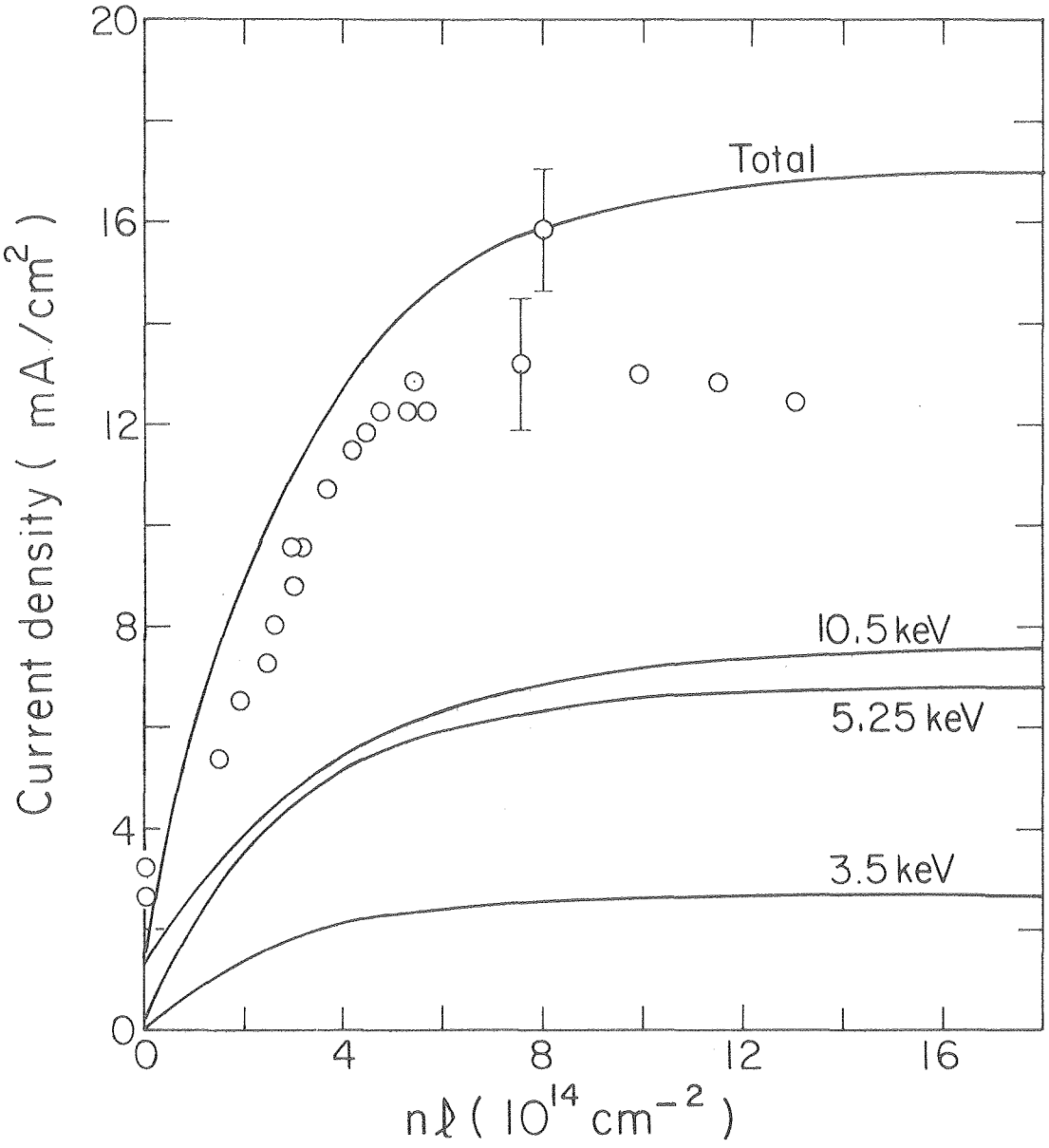

Fig. 10

XBL 805-1010A

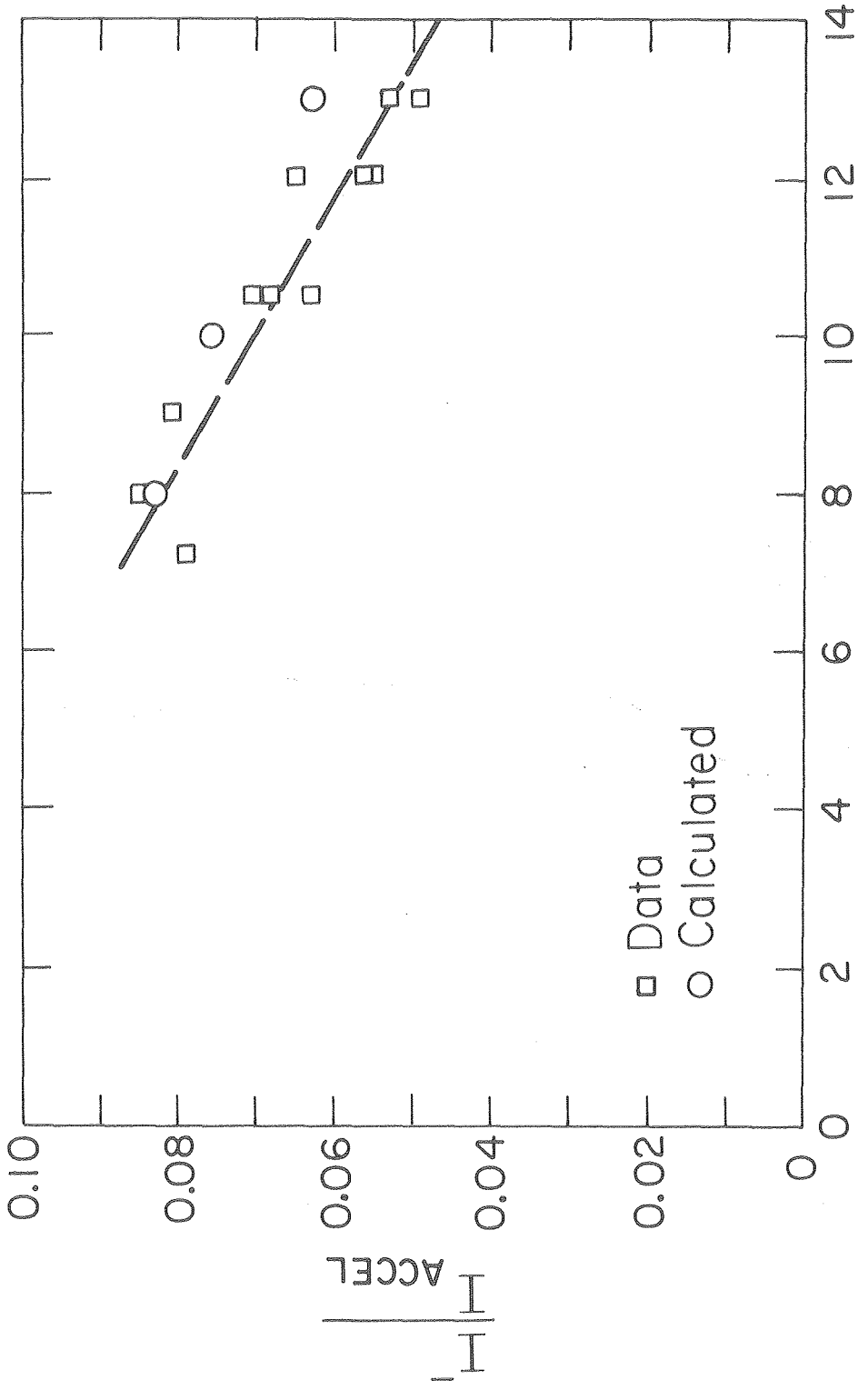

XBL 806-1026

Fig. 11

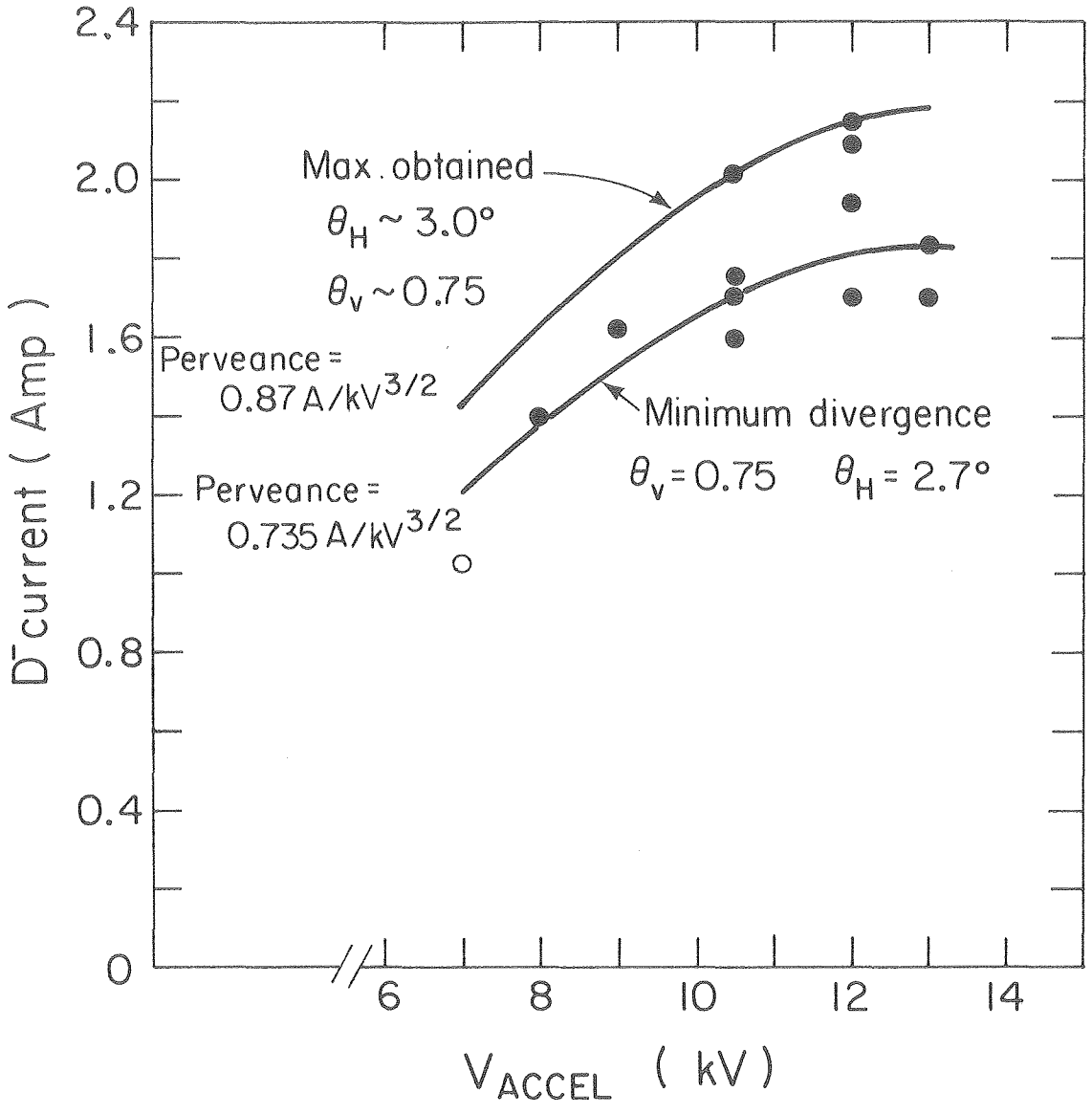

Fig. 12

XBL 806-1023

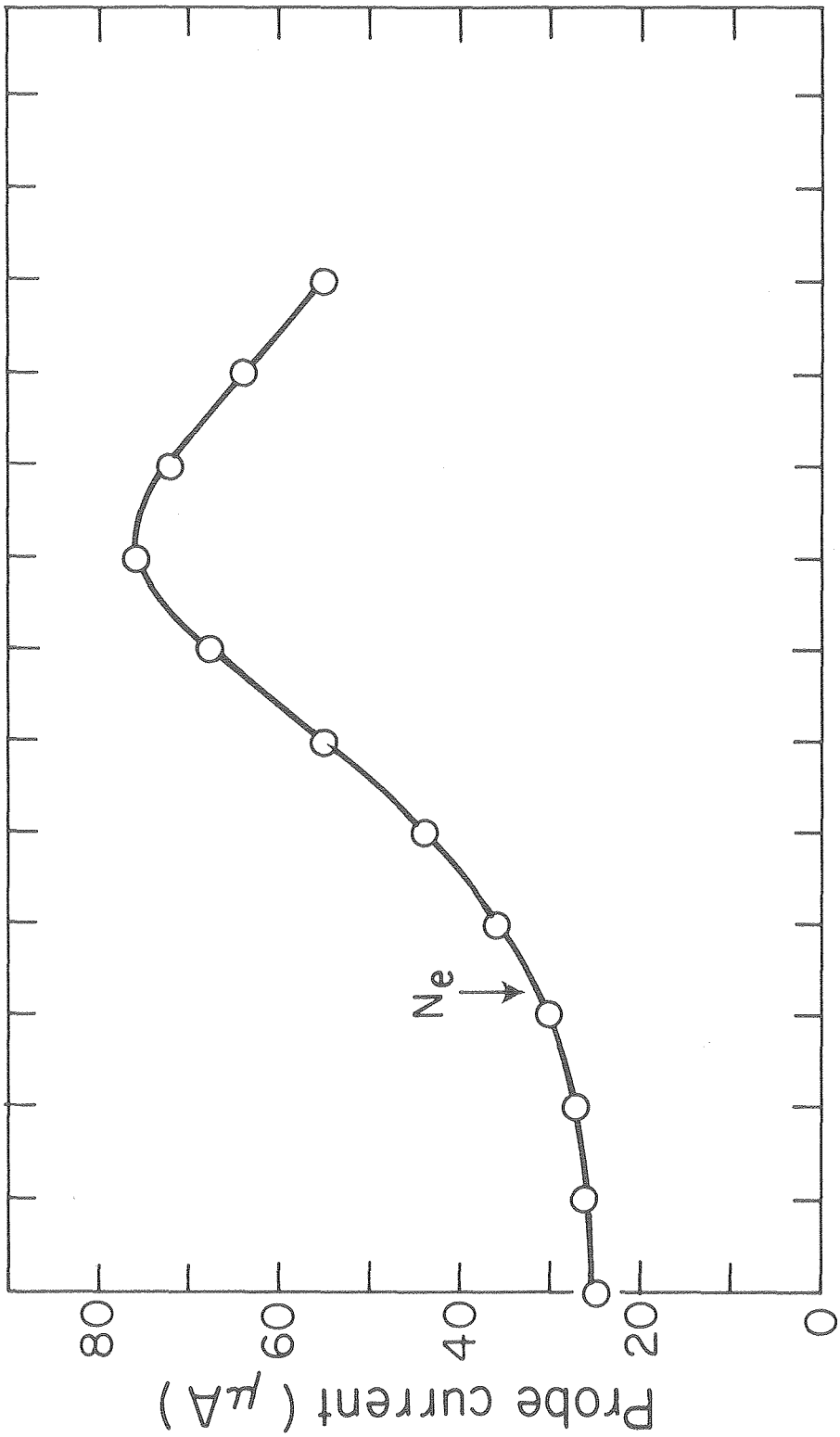

XBL 806-1015

Fig. 13

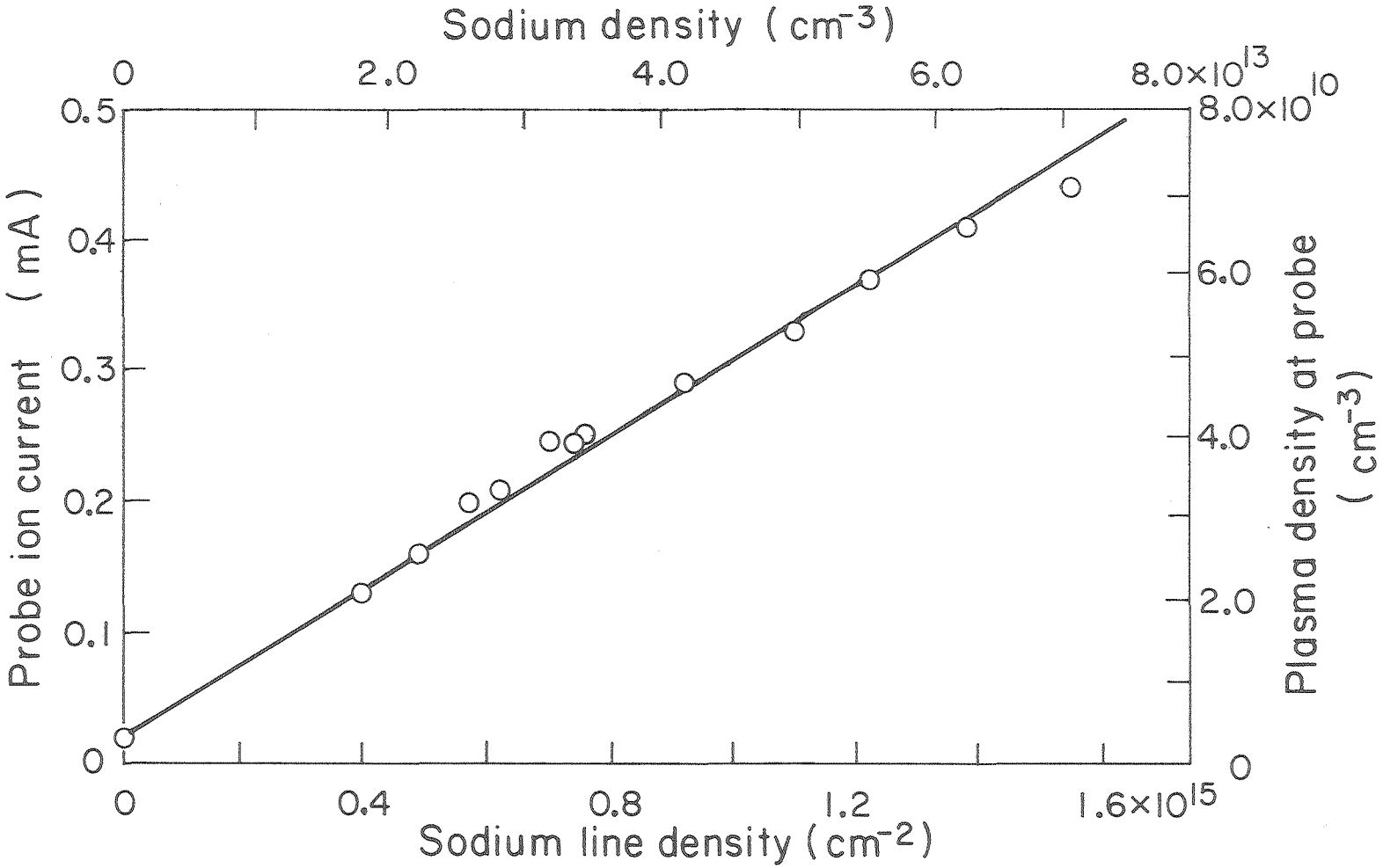

Fig. 14

XBL 806-1014

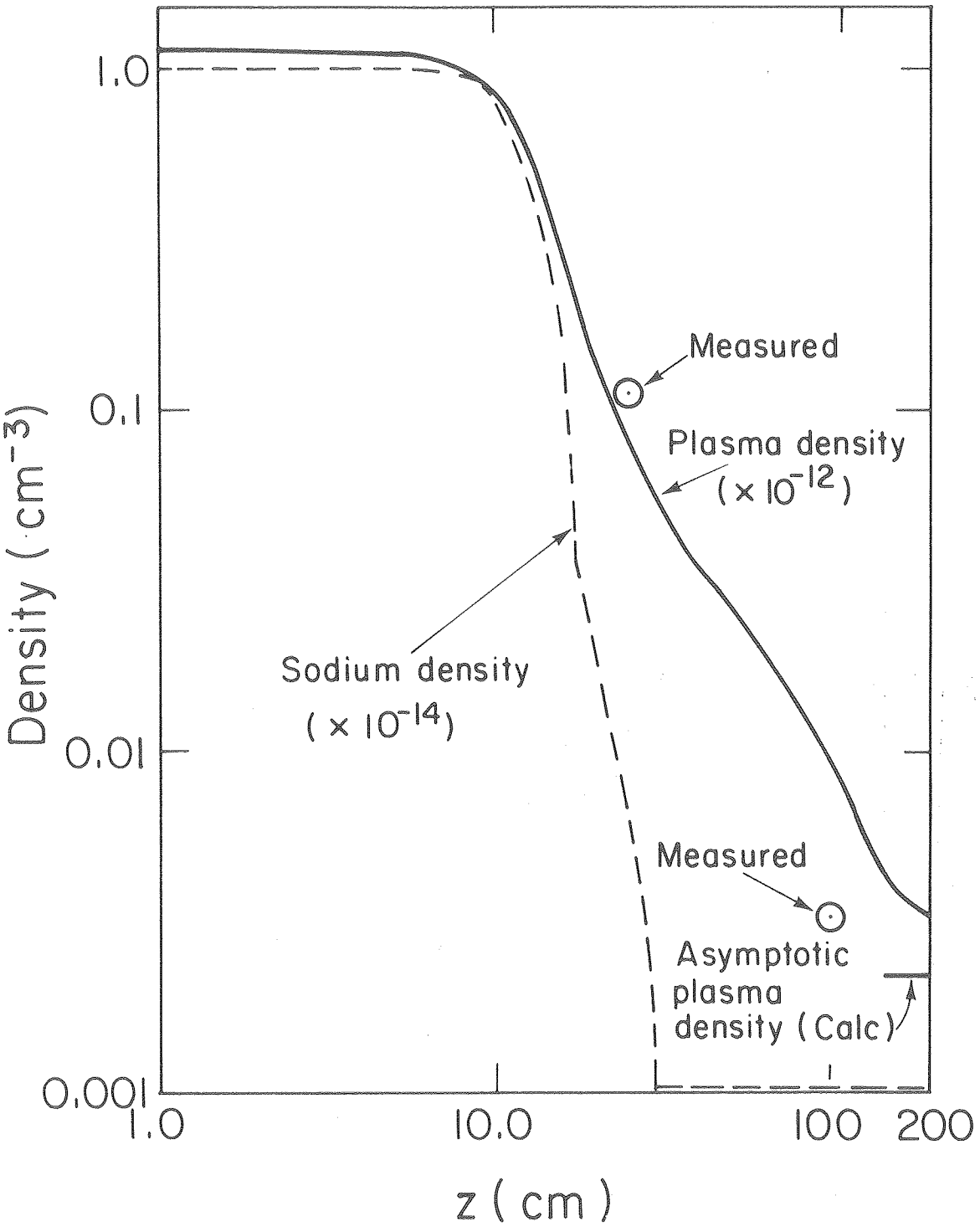

Fig. 15

XBL 805-1011

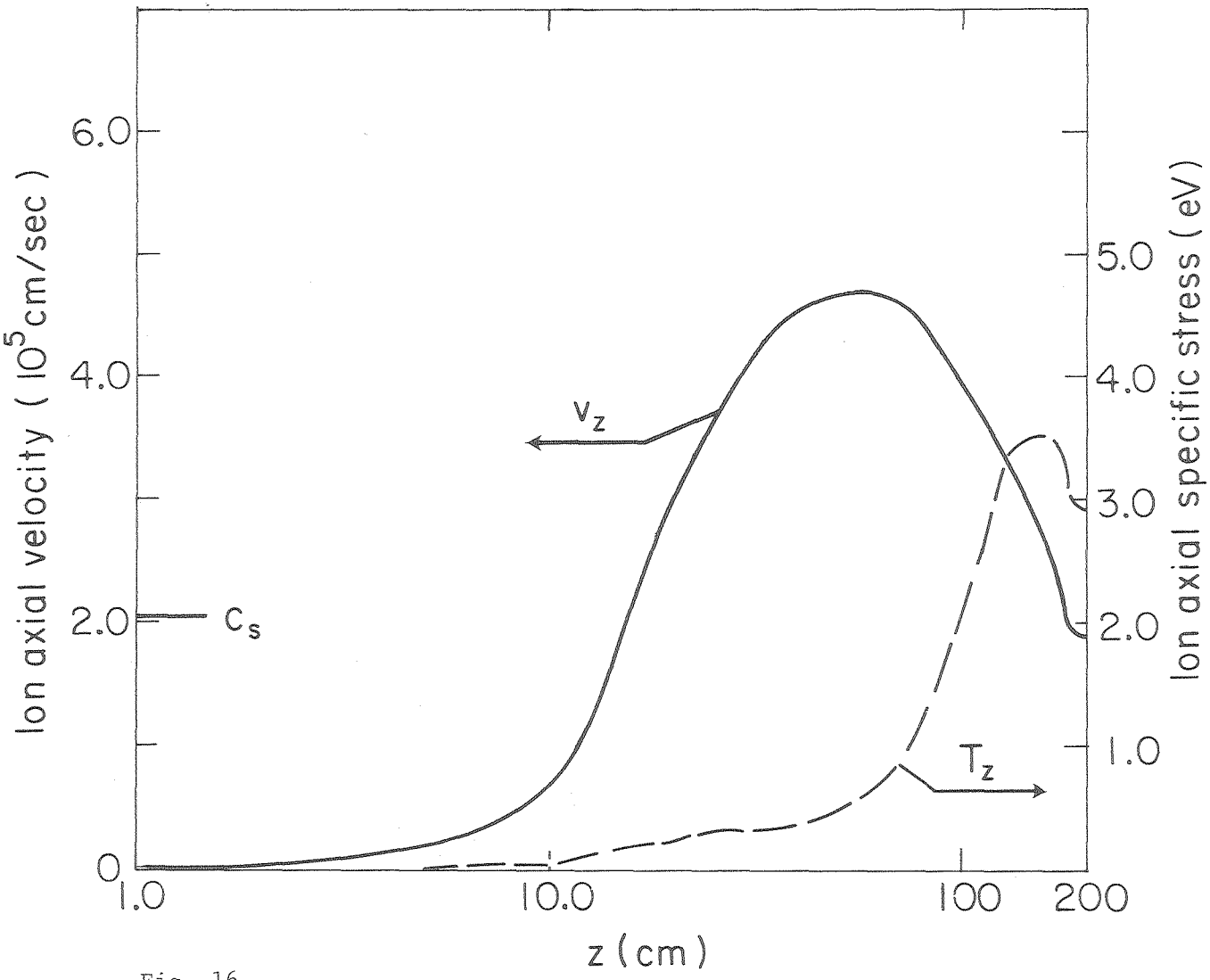

Fig. 16

XBL 806-1012A

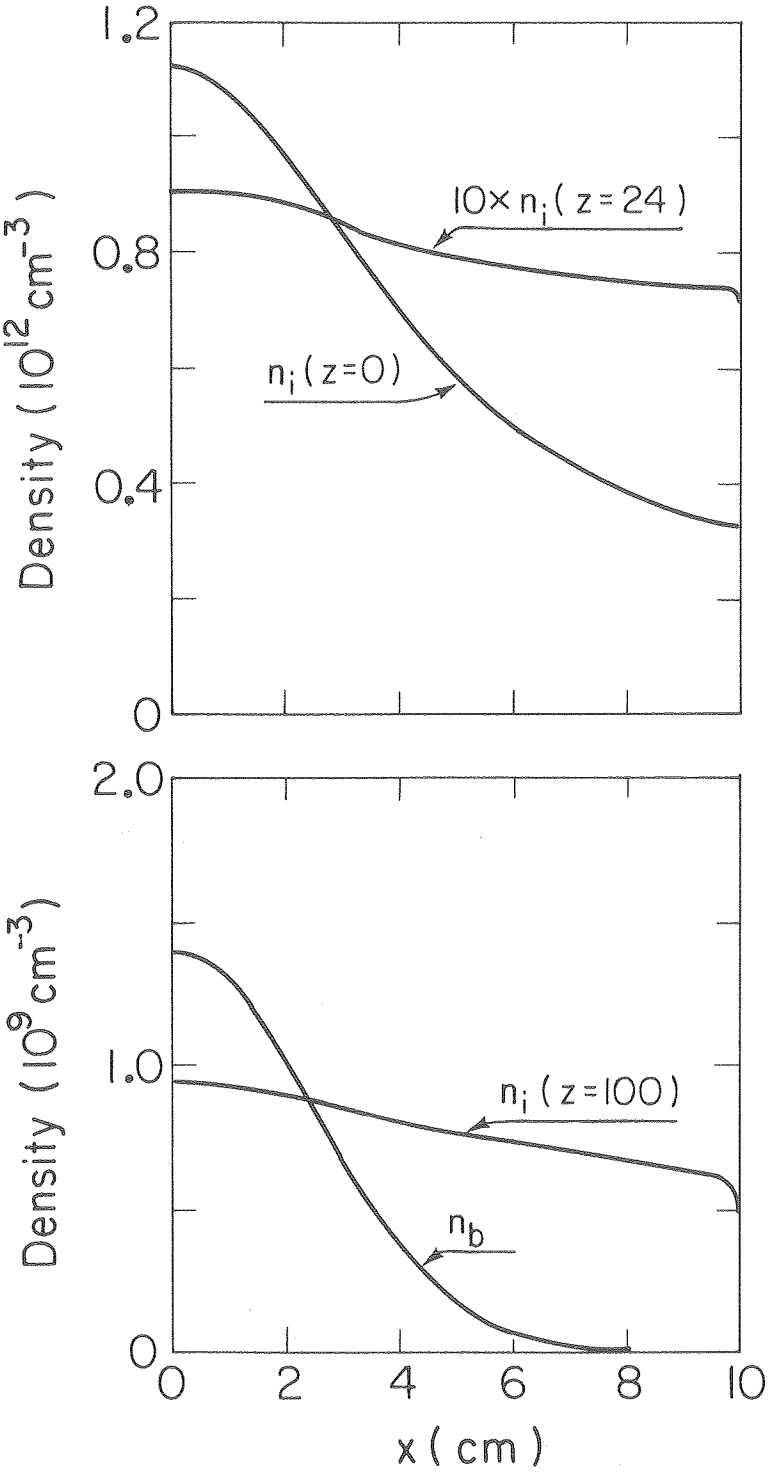

Fig. 17

XBL 806-1017

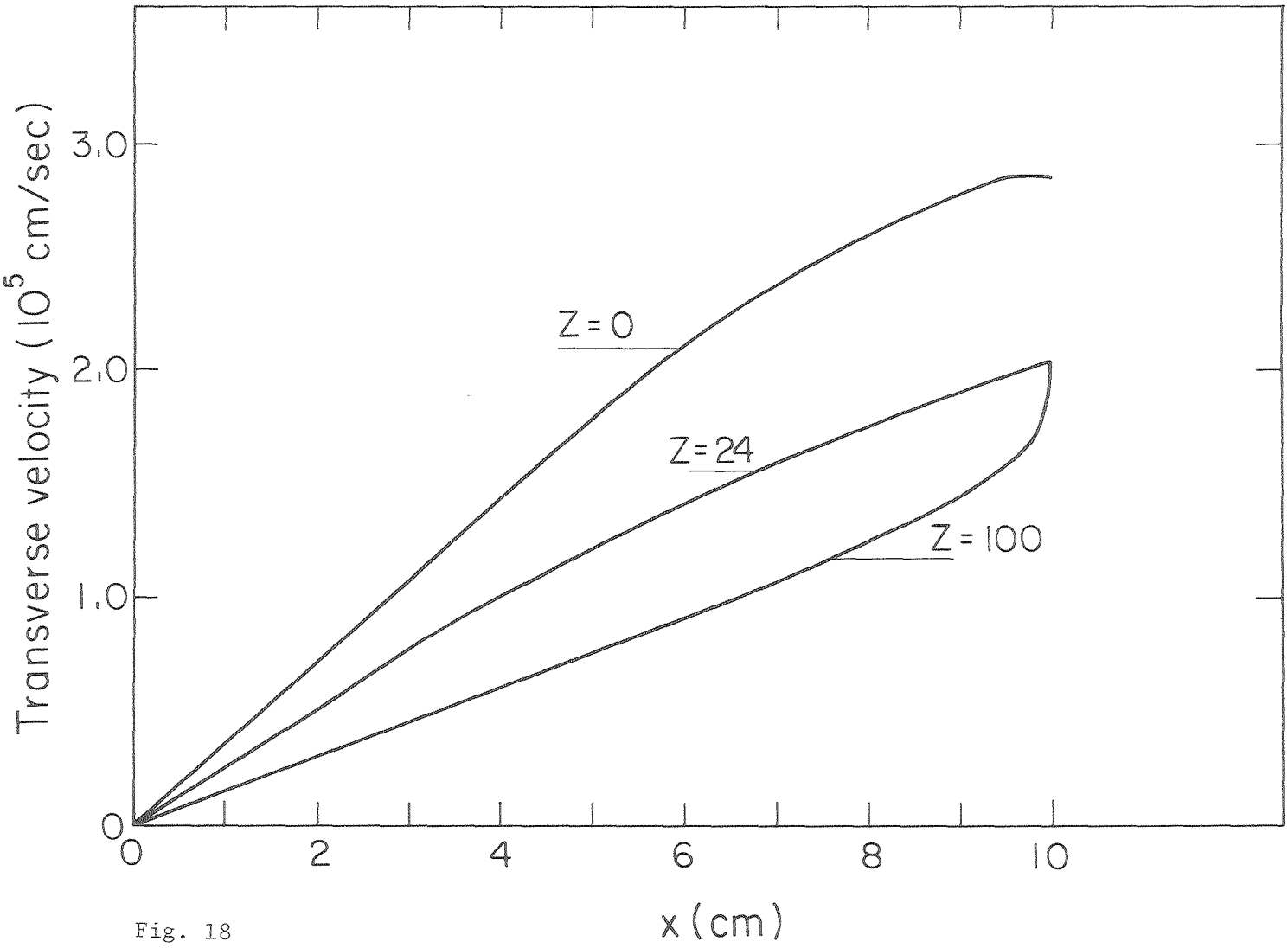

Fig. 18

XBL 805-1009

TECHNICAL INFORMATION DEPARTMENT
LAWRENCE BERKELEY LABORATORY
UNIVERSITY OF CALIFORNIA
BERKELEY, CALIFORNIA 94720